© 2020. Published by The Company of Biologists Ltd | Journal of Cell Science (2020) 133, jcs237776. doi:10.1242/jcs.237776

RESEARCH ARTICLE

Sex differences in the proliferation of pulmonary artery endothelial cells: implications for plexiform arteriopathy

Shanshan Qin[1], Dan N. Predescu[1], Monal Patel[2], Patrick Drazkowski[1], Balaji Ganesh[3] and Sanda A. Predescu[1,*]

ABSTRACT

The sex-biased disease pulmonary arterial hypertension (PAH) is characterized by the proliferation and overgrowth of dysfunctional pulmonary artery endothelial cells (PAECs). During inflammation associated with PAH, granzyme B cleaves intersectin-1 to produce N-terminal (EH_{ITSN}) and C-terminal (SH3A–E_{ITSN}) protein fragments. In a murine model of PAH, EH_{ITSN} triggers plexiform arteriopathy via p38–ELK1–c-Fos signaling. The SH3A–E_{ITSN} fragment also influences signaling, having dominant-negative effects on ERK1 and ERK2 (also known as MAPK3 and MAPK1, respectively). Using PAECs engineered to express tagged versions of EH_{ITSN} and SH3A–E_{ITSN}, we demonstrate that the two ITSN fragments increase both p38–ELK1 activation and the ratio of p38 to ERK1 and ERK2 activity, leading to PAEC proliferation, with female cells being more responsive than male cells. Furthermore, expression of EH_{ITSN} substantially upregulates the expression and activity of the long non-coding RNA *Xist* in female PAECs, which in turn upregulates the X-linked gene *ELK1* and represses expression of *krüppel-like factor 2* (*KLF2*). These events are recapitulated by the PAECs of female idiopathic PAH patients, and may account for their proliferative phenotype. Thus, upregulation of *Xist* could be an important factor in explaining sexual dimorphism in the proliferative response of PAECs and the imbalanced sex ratio of PAH.

KEY WORDS: Intersectin, Endothelial cells, Proliferation, Plexiform phenotype, p38 to ERK1/2 activity ratio, Sexual dimorphism, ELK1, c-Fos, lncRNA *Xist*, KLF2

INTRODUCTION

Intersectin-1s (a short isoform of intersectin-1, referred to here as ITSN), first identified as an endocytic protein and a potential connection between endocytosis and exocytosis, has a wide range of physiological and pathological functions. ITSN participates in scaffolding of the endocytic machinery, regulation of dynamin-2 function, formation of endocytic vesicles and coordination of endocytic membrane traffic with actin assembly (Okamoto et al., 1999; Hussain et al., 1999; Predescu et al., 2003). Moreover, dysregulated ITSN expression has been implicated in several human cancers, lung injury, pulmonary arterial hypertension (PAH) and neurodegenerative disorders such as Down syndrome and Alzheimer's disease (Keating et al., 2006; Harris et al., 2017; Russo et al., 2015; Gu et al., 2015; Jeganathan et al., 2016; Patel et al., 2017; Shah et al., 2018). ITSN regulates a variety of signaling pathways, including those involving Ras, TGFβR1 (also known as TGFBR1, or ALK5), receptor tyrosine kinases and MAPKs, as part of diverse processes including neuronal migration, synaptic plasticity, learning and memory (Hunter et al., 2013; Jeganathan et al., 2017; Alvisi et al., 2018; Jakob et al., 2017; Sengar et al., 2013). Initially thought to be a cytoplasmic membrane-associated protein, ITSN has also been found to localize to the nucleus (Alvisi et al., 2018; Okamoto et al., 1999). Intersectin-1 is a ubiquitously expressed protein, encoded by a gene located on chromosome 21 (21q22.11), with two main protein isoforms and multiple known mRNA splice variants (Kropyvko et al., 2010; Pucharcos et al., 2001). ITSN has several important functional domains: an N-terminal domain composed of two epsin15 homology motifs (EH1–EH2), a central coiled-coil domain and a C-terminal domain comprising five consecutive src homology-3 motifs (SH3A–E_{ITSN}). The different domains of ITSN mediate multiple protein–protein interactions. ITSN interacts with epsin-1, epsin-2, stonin-2, RAB/Rip (also known as AGFG1), IGFBP1 and IGFBP2 via the EH domains. The coiled-coil domain of ITSN binds SNAP23, SNAP25 and epsin, whereas the SH3A–E region mediates the interactions of ITSN with dynamin, synaptojanin-1, CDGAP (also known as ARHGAP31), N-WASP and son of sevenless homolog 1 (SOS1) (Gardiner et al., 2004). Moreover, within the EH2 domain there is a well-conserved granzyme B (GrB) cleavage site, $IDQD^{271}GK$ (Patel et al., 2013; Loeb et al., 2006). Under inflammatory conditions associated with PAH, GrB cleaves ITSN and generates EH_{ITSN}, a biologically active protein fragment with endothelial cell (EC) proliferative potential, which is mediated via sustained activation of the MAPK p38, the transcription factor ELK1 and the immediate-early response gene *c-Fos* (also known as *FOS*) (Patel et al., 2013). Prolonged expression of EH_{ITSN} in the lungs of ITSN-knockout heterozygous mice results in a severe lung phenotype characterized by occlusive proliferation of ECs and formation of plexiform lesions as well as differences in function of the right ventricle. This phenotype closely recapitulates many of the characteristics of human PAH, including gender differences (Patel et al., 2017; Predescu et al., 2019).

We have previously reported that expression of EH_{ITSN}, in a similar manner to ITSN deficiency, can shift physiological (caveolae-mediated) vesicular transport towards alternative endocytic pathways, a finding that further supports the idea that ITSN has a significant role in the dysfunctional molecular phenotype of PAECs in PAH (Predescu et al., 2018). The SH3A–E_{ITSN} fragment functions in a dominant-negative manner by sequestering the interacting partners of ITSN (specifically dynamin and SOS1) away from their sites of action, with detrimental consequences for

[1]Department of Internal Medicine, Pulmonary, Critical Care and Sleep Medicine, Rush University Medical Center, Chicago, IL 60612, USA. [2]Division of Hematology/Oncology, Feinberg School of Medicine, Northwestern University, Chicago, IL 60611, USA. [3]Division of Bioanalytics, Biophysics and Cytomics, University of Illinois at Chicago, Chicago, IL 60612, USA.

*Author for correspondence (Sanda_Predescu@rush.edu)

S.A.P., 0000-0002-9386-6756

Handling Editor: John Heath
Received 8 August 2019; Accepted 13 March 2020

Journal of Cell Science (2020) 133, jcs237776. doi:10.1242/jcs.237776

endocytosis and pro-survival signaling via ERK1 and ERK2 (also known as MAPK3 and MAPK1, respectively, and referred to hereafter collectively as ERK1/2) (Tong et al., 2000b). As proteolysis of ITSN by GrB generates two biologically active protein fragments, the N-terminal EH_{ITSN} and the C-terminal SH3A–E_{ITSN}, we sought to gain more insight into the proliferative effects of EH_{ITSN} activity and to determine how interplay between the two concurrently expressed protein fragments affects EC proliferation and endocytic activity. Here, we report that, despite the dominant-negative effects of the SH3A–E_{ITSN} fragment, EH_{ITSN} is still able to contribute to the endocytic activity, proliferation and overgrowth of dysfunctional PAECs, and hence influence the development and progression of PAH. The concurrent expression of the two protein fragments augmented the activation of p38–ELK1 and increased the ratio of p38 to ERK1/2 activity, with female cells being more responsive than male cells. Moreover, the increased responsiveness of female cells to EH_{ITSN} expression is due to upregulation (above basal levels) of expression of the long non-coding RNA (lncRNA) *Xist* (X-inactive specific transcript), which is essential for X-chromosome inactivation and dosage compensation of expression of X-linked genes (Yang et al., 2018). Downregulation of *Xist* gene expression using siRNA, or by inhibition using a highly specific EH_{ITSN} inhibitory peptide, causes a decrease in proliferation of PAECs and inhibits activation of p38–ELK1–c-Fos signaling. Moreover, *Xist* upregulation augments the expression of *ELK1*, an X-linked gene implicated in PAH pathobiology, and negatively regulates expression of *KLF2*, which encodes a key transcription factor that governs signaling pathways regulating the EC dysfunction that characterizes PAH (McLean et al., 2012). These molecular alterations could explain sexual dimorphism in the proliferative potential of PAECs, and the higher susceptibility of women to PAH.

RESULTS

EH_{ITSN} and SH3A–E_{ITSN} can be efficiently expressed in cultured PAECs

To address the effects of concurrent expression of the two ITSN protein fragments on EC phenotype, and to determine whether the proliferative potential of EH_{ITSN} is affected by the presence of SH3A–E_{ITSN}, we cloned the EH_{ITSN} cDNA into myc- and GFP-tag expression vectors, and cloned the SH3A–E_{ITSN} cDNA into FLAG- and mCherry-tag expression vectors. A schematic of the domain structure of ITSN and the site of GrB cleavage is illustrated in Fig. 1A. The two ITSN protein fragments were expressed individually or together in human PAECs. Following optimization of transfection conditions, analyses of cell lysates by western blotting using myc and FLAG antibodies demonstrated efficient expression of the two ITSN protein fragments at 48 h post-transfection (Fig. 1B). No tag immunoreactivity was detected in untreated control cells (Fig. 1B). Demonstration of equivalent expression levels for the two protein fragments in co-transfected cells was not feasible by western blotting, as two different tag antibodies with different characteristics were used.

Direct fluorescence imaging of GFP-EH_{ITSN}- and mCherry-SH3A–E_{ITSN}-transfected cells (Fig. 1C,D) further demonstrated efficient protein expression. When expressed individually, GFP-EH_{ITSN} was found in the cytosol, at the plasma membrane and often within the nucleus (Fig. 1C), whereas mCherry-SH3A–E_{ITSN} was found mainly in the cytosol (Fig. 1D). Co-transfected cells showed proximity between the two protein fragments and a certain degree of colocalization (Fig. 1E), as well as a more limited plasma membrane distribution (Fig. 1E, arrows). DAPI staining of EC nuclei, as an indicator of the total cell population, was used to quantify the transfection efficiency expressed as the ratio of the number of fluorescent tag-positive cells versus the total number of cells. We found an average transfection efficiency of 65–70% for the experimental conditions used (Fig. 1F). To document the efficient transfection and subcellular distribution of GFP-EH_{ITSN} and mCherry-SH3A–E_{ITSN} in cultured PAECs, lower magnification micrographs are included in Fig. S1. Given the proliferative potential of EH_{ITSN} and its nuclear localization, we subjected myc-EH_{ITSN}-transfected male and female PAECs to subcellular fractionation, as described by Patel et al. (2013), to quantitatively evaluate the subcellular distribution of this fragment. The nuclear and cytosolic fractions, pre-cleared with Protein A/G, were subjected to immunoprecipitation with myc antibodies followed by western blot analyses using an antibody against the ITSN EH domains (Fig. 1G). Myc-EH_{ITSN} was found to be distributed in both the cytoplasm and the nucleus, in a ratio of 3:1, as determined by densitometry, with no significant differences between female and male fractions (Fig. 1G). No myc-EH_{ITSN} immunoreactivity was detected in non-transfected control PAECs ($PAEC_{Ctrl}$; Fig. 1G). Omission of the myc antibody from the immunoprecipitation reaction was used as a negative control (data not shown).

Concurrent expression of EH_{ITSN} and SH3A–E_{ITSN} does not affect the increased endocytic activity of EH_{ITSN}-expressing PAECs

Based on the findings of previous studies into the functional impact of individually expressed EH_{ITSN} and SH3A–E_{ITSN} fragments on the endocytic activity of ECs, we decided to investigate the effects of simultaneous expression of the two fragments. To this intent, control and transfected PAECs were subjected to a biotin-based assay of caveolae internalization that used fluorescent labeling by Alexa-Fluor-594-conjugated NeutrAvidin to detect internalized biotinylated proteins, as described by Predescu et al. (2003). For all cell lines tested ($PAEC_{Ctrl}$, myc-EH_{ITSN}-transfected PAECs, FLAG-SH3A–E_{ITSN}-transfected PAECs and myc-EH_{ITSN} and FLAG-SH3A–E_{ITSN} co-transfected cells), this assay revealed fine fluorescent puncta at the cell surface and scattered fluorescent puncta all over the cytoplasm (Fig. 2A–D), with no significant differences between cell lines in the pattern of NeutrAvidin–Alexa Fluor 594 labeling. However, this fine punctate labeling, indicative of biotin association with endothelial vesicular carriers, was less pronounced in all transfected cells due to impairment of vesicular (caveolae-mediated) transport. As expected, the frequency of large fluorescent puncta showed a modest increase in all transfected cells compared to $PAEC_{Ctrl}$ (Fig. 2B–D, arrowheads). This increase in large puncta is consistent with the ability of ECs to upregulate morphological intermediates (large endocytic structures, membranous rings, and vesiculo-tubular elements) of compensatory endocytic pathways when caveolae-mediated transport is impaired. In our cellular context, the impairment in vesicular transport is likely due to either the lack of the peripheral actin band, as caused by EH_{ITSN} expression, or sequestration of dynamin-2 in the cytosol, away from the neck region of caveolae, as caused by SH3A–E_{ITSN} expression, or a combination of these two effects (Predescu et al., 2003, 2018).

Quantification of internalized biotin by ELISA using streptavidin–horseradish peroxidase (HRP) indicated a 28% increase in biotin uptake in myc-EH_{ITSN}-transfected PAECs compared to biotin uptake in untreated PAECs (Fig. 2E). FLAG-SH3A–E_{ITSN}-transfected PAECs showed ∼20% inhibition of biotin uptake, while the double-transfected PAECs showed a biotin uptake similar to that of EH_{ITSN}-expressing cells (Fig. 2E). This observation indicates that the functional upregulation of

Journal of Cell Science (2020) 133, jcs237776. doi:10.1242/jcs.237776

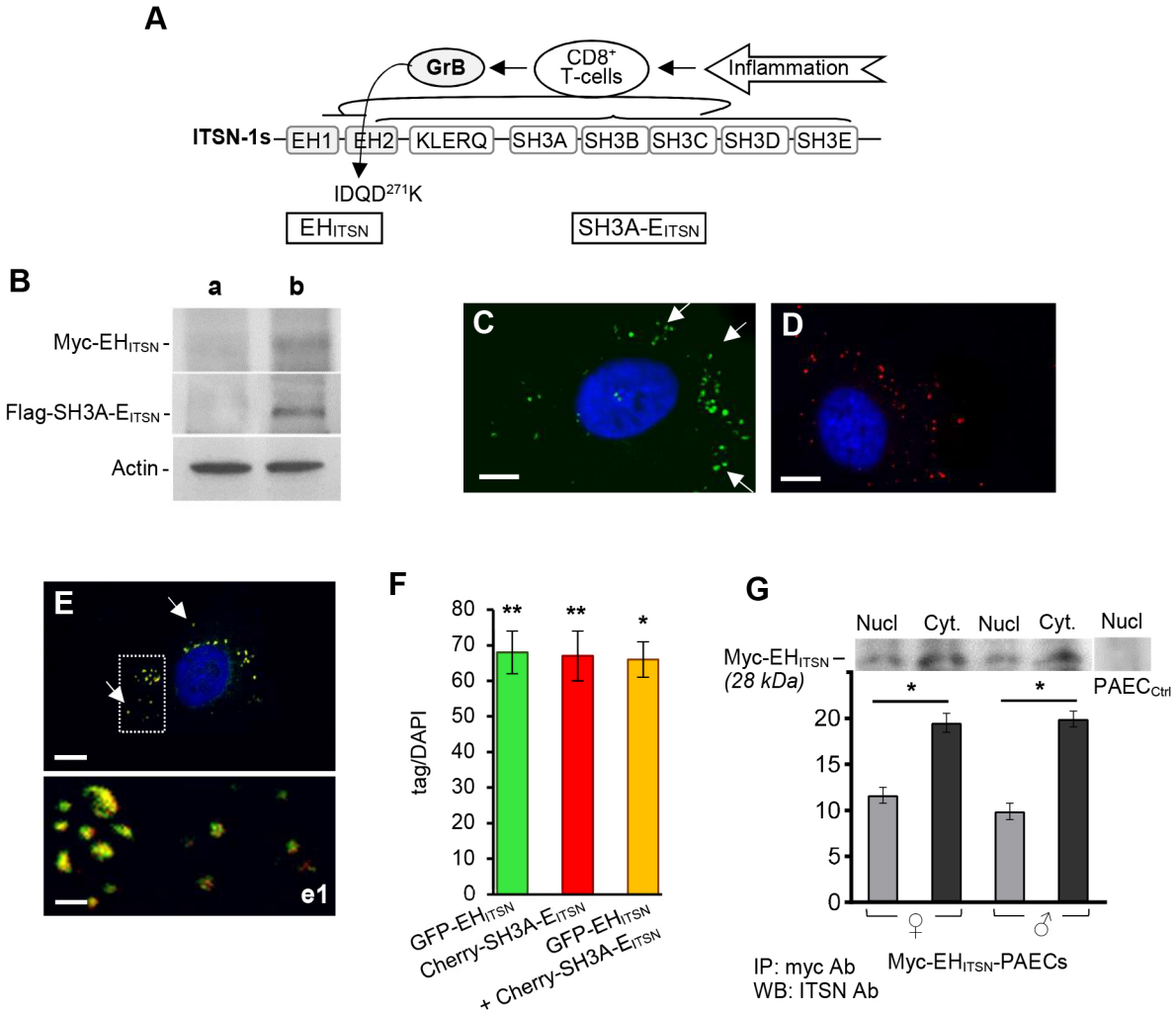

Fig. 1. EH_{ITSN} and $SH3A–E_{ITSN}$ cDNA plasmids are efficiently expressed in cultured PAECs. (A) Diagram showing the domain structure of ITSN and GrB cleavage. Within the EH2 domain of ITSN there is a single, well-conserved GrB cleavage site, $IDQD^{271}GK$. (B) Lysates (70 µg/lane) of control (a) and myc-EH_{ITSN}- and FLAG-SH3A–E_{ITSN}-transfected PAECs (b) were subjected to SDS–PAGE and western blotting using anti-myc and anti-FLAG antibodies. Actin is shown as a loading control. (C–E) Imaging analyses of expression and subcellular distribution of GFP-EH_{ITSN} and mCherry-SH3A–E_{ITSN}. A cell expressing GFP-EH_{ITSN} is shown in C, and a cell expressing mCherry-SH3A–E_{ITSN} is shown in D. Panel E and magnification e1 show the proximity of the two protein fragments in PAECs co-transfected with the two plasmids. The dashed box in E indicates the location of magnification e1. Arrows in C and E indicate punctate signal localized at the plasma membrane. (F) The transfection efficiency of PAECs was determined as the ratio of cells expressing the fluorescent tag (GFP, mCherry or GFP and mCherry) versus the total number of cells (determined by DAPI staining) across 50 high power fields of view. Data are expressed as mean±s.d. n=3 independent experiments, performed in triplicates. *P<0.05; **P<0.01. The P values for each condition were obtained by comparing the number of tag-positive cells to the number of DAPI-stained cells. (G) Quantification and representative western blot of the subcellular distribution of myc-EH_{ITSN} in transfected female and male PAECs. Nuclear (Nucl) and cytosolic (Cyt.) fractions (350 µg total protein) were pre-cleared with Protein A/G, followed by incubation with anti-myc antibody and protein A/G. Western blotting for detection of the myc-EH_{ITSN} was performed with an ITSN antibody that recognized an EH epitope. No myc-EH_{ITSN} immunoreactivity is detected in non-transfected $PAEC_{Ctrl}$. Densitometry was performed on representative x-ray films with identical chemiluminescent detection conditions. Data are expressed as mean±s.d. n=3. *P<0.01. Scale bars: 10 µm (C–E), 3 µm (e1).

compensatory transport pathways induced by expression of the two ITSN fragments accounts for a highly efficient endocytic activity, demonstrating a potential role for the concurrent expression of EH_{ITSN} and $SH3A–E_{ITSN}$ in the proliferation and overgrowth of PAECs in PAH, and thus, in the development of the disease.

$SH3A–E_{ITSN}$ does not prevent EH_{ITSN} from exerting its proliferative potential in ECs

Next, we used flow cytometry analyses of the cell cycle to evaluate whether the proliferative potential of EH_{ITSN} in PAECs is affected by expression of $SH3A–E_{ITSN}$. For these analyses, PAECs were transfected with GFP-EH_{ITSN}, and mCherry-$SH3A–E_{ITSN}$ plasmids, either singly or in combination. At 48 h post-transfection, PAECs were stained with the nucleic acid stain DAPI and used in flow cytometry analyses of cellular DNA content (Fig. 3A–C). Estimates of the percentage of proliferating cells in the entire PAEC population indicated that $SH3A–E_{ITSN}$ expression caused a decrease of ∼26% in the proportion of proliferating cells relative to that in the total EH_{ITSN} population (Fig. 3D), whereas concurrent expression of EH_{ITSN} and $SH3A–E_{ITSN}$ resulted in a decrease of only 12% (Fig. 3D), suggesting that, despite the dominant-negative effects of the $SH3A–E_{ITSN}$ on ERK1/2 pro-survival signaling (Tong et al., 2000a), EH_{ITSN} still maintained its proliferative potential. Similar results were obtained when only transfected PAECs were analyzed.

Journal of Cell Science (2020) 133, jcs237776. doi:10.1242/jcs.237776

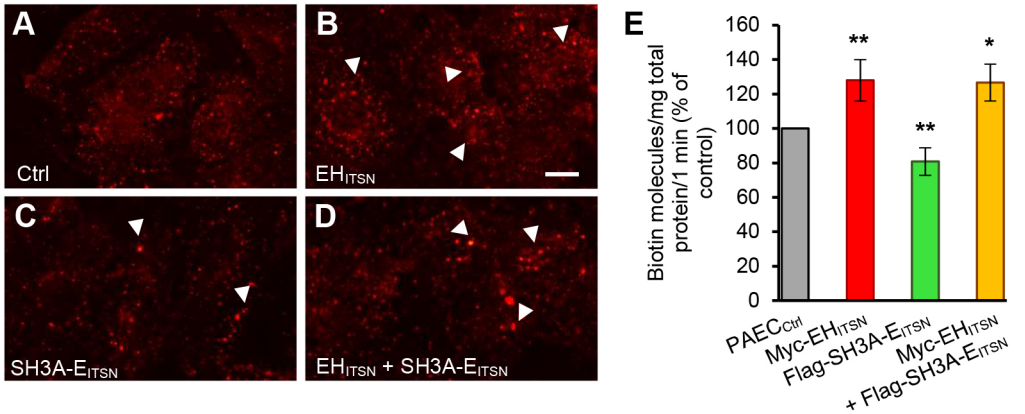

Fig. 2. Concurrent expression of EH_{ITSN} and SH3A–E_{ITSN} does not affect the increased endocytic activity of myc-EH_{ITSN} expressing PAECs. $PAEC_{Ctrl}$ (A) and PAECs transfected with myc-EH_{ITSN} (B), FLAG-SH3A–E_{ITSN} (C) or myc-EH_{ITSN} and FLAG-SH3A–E_{ITSN} (D) were subjected to biotinylation of cell surface proteins at 48 h post-transfection, followed by biotin internalization and NeutrAvidin Dylight 495 staining. Arrowheads indicate large fluorescent puncta. (E) Quantification of internalized biotin, as assayed by an ELISA using streptavidin-HRP, in $PAEC_{Ctrl}$ and transfected cells as indicated and expressed relative to $PAEC_{Ctrl}$, which was normalized to 100. Results are the mean±s.d. of eight different experiments each performed in triplicate. *P<0.01, **P<0.001. Images in A–D were taken at the same magnification. Scale bar: 10 µm.

At 48 h post-transfection, SH3A–E_{ITSN} expression reduced the number of proliferating cells by ∼30% (from 15.5×10^3 to 10.8×10^3), while concurrent expression of EH_{ITSN} and SH3A–E_{ITSN} caused a decrease in the number of proliferating PAECs of only ∼13% (from 15.5×10^3 to 13.4×10^3) (Fig. 3E,F). These data indicate that PAECs that express the two ITSN fragments at the same time have a proliferation rate comparable to that of cells expressing EH_{ITSN} only, and thus SH3A–E_{ITSN} does not prevent EH_{ITSN} from exerting its proliferative potential.

PAECs show gender differences in the proliferative response to EH_{ITSN} expression

To further investigate the proliferative response to EH_{ITSN} expression, control PAECs and PAECs transfected as above, were subjected to an EdU-based cell proliferation assay and DAPI counterstaining (Fig. 3G–J). Because the physiology and pathology of PAECs are involved in gender difference in PAH, we used PAECs from both male and female donors to evaluate whether these cultured human PAECs show differences in their proliferative response to the expression of ITSN fragments. Manual counting of EdU-positive cells and DAPI counterstained cells at 48 h post-transfection indicated that, for all experimental conditions tested, female PAECs show a higher proliferation rate compared to that of male PAECs (Fig. 3K). When female PAECs were analyzed, we observed that EH_{ITSN} expression caused a 37% increase in the proportion of EdU-positive PAECs compared to that observed in non-transfected PAECs. PAECs transfected with SH3A–E_{ITSN} showed a 12% reduction in proliferation compared to control cells and a 25% inhibition compared to myc-EH_{ITSN}-transfected PAECs. In PAECs concurrently expressing the two ITSN protein fragments, the proportion of EdU-positive cells was close to that observed for GFP-EH_{ITSN}-transfected cells. Male PAECs showed a similar trend in their proliferative response to the expression of the two protein fragments, but they are less responsive overall (Fig. 3K and Table S1). Transfection with the empty vector did not affect the number of EdU-positive PAECs by reference to controls (not shown). These data further demonstrate that SH3A–E_{ITSN} does not prevent EH_{ITSN} from exerting its proliferative potential and show that there are gender differences in the proliferative response of PAECs to EH_{ITSN} expression, with PAECs from the female donor having a higher proliferation rate than PAECs from the male donor.

Concurrent expression of the two protein fragments increases the ratio of p38 to ERK1/2 activity ratio

As our previous studies indicated that myc-EH_{ITSN} expression in mouse lungs triggers a p38–ELK1–c-Fos proliferative signaling response responsible for EC proliferation and plexogenic arteriopathy (Patel et al., 2017), with a more severe lung phenotype in female mice (Predescu et al., 2019), we next addressed whether concurrent expression of the two ITSN fragments affects p38 phosphorylation. Lysates from female-donor PAECs transfected with myc-EH_{ITSN}, FLAG-SH3A–E_{ITSN} and myc-EH_{ITSN} and FLAG-SH3A–E_{ITSN} combined, alongside untransfected control lysates ($PAEC_{Ctrl}$), were subjected to western blotting with antibodies that recognize phosphorylated and total p38 kinase (Fig. 4A). Densitometric analysis indicated that myc-EH_{ITSN} expression induced a greater than 2-fold increase in p38 phosphorylation, compared to the level in $PAEC_{Ctrl}$ (Fig. 4A). A similar increase in phosphorylated p38 was detected in PAECs transfected with both EH_{ITSN} and SH3A–E_{ITSN}, whereas cells only transfected with SH3A–E_{ITSN} showed only 1.9-fold increase in p38 phosphorylation. As the expression of SH3A–E_{ITSN} was expected to inhibit ERK1/2 activation, and because previous studies indicate that p38 signaling causes rapid inactivation of ERK1/2 through PP2A activation (Juntilla and Koretzky, 2008), we next analyzed ERK1/2 phosphorylation status. Although expression of EH_{ITSN} caused ∼20% decrease in ERK1/2 phosphorylation, the expression of SH3A–E_{ITSN} induced a significant decrease of 50% (Fig. 4B). Concurrent expression of the two cleavage fragments of ITSN also resulted in a 50% decrease in ERK1/2 phosphorylation, consistent with previous reports regarding negative regulation of the ERK1/2 pathway through p38 signaling. Because the balance of ERK1/2 and p38 kinase activity may play a crucial role in regulation of the cell cycle (Zhang and Liu, 2002), we also evaluated the effects of EH_{ITSN} and SH3A–E_{ITSN} concurrent expression on the ratio of p38 to ERK1/2 activity (Fig. 4C). These data are consistent with a model wherein concurrent expression of the two protein fragments produces a high ratio of p38 to ERK1/2 activity, which favors EC proliferation.

Journal of Cell Science (2020) 133, jcs237776. doi:10.1242/jcs.237776

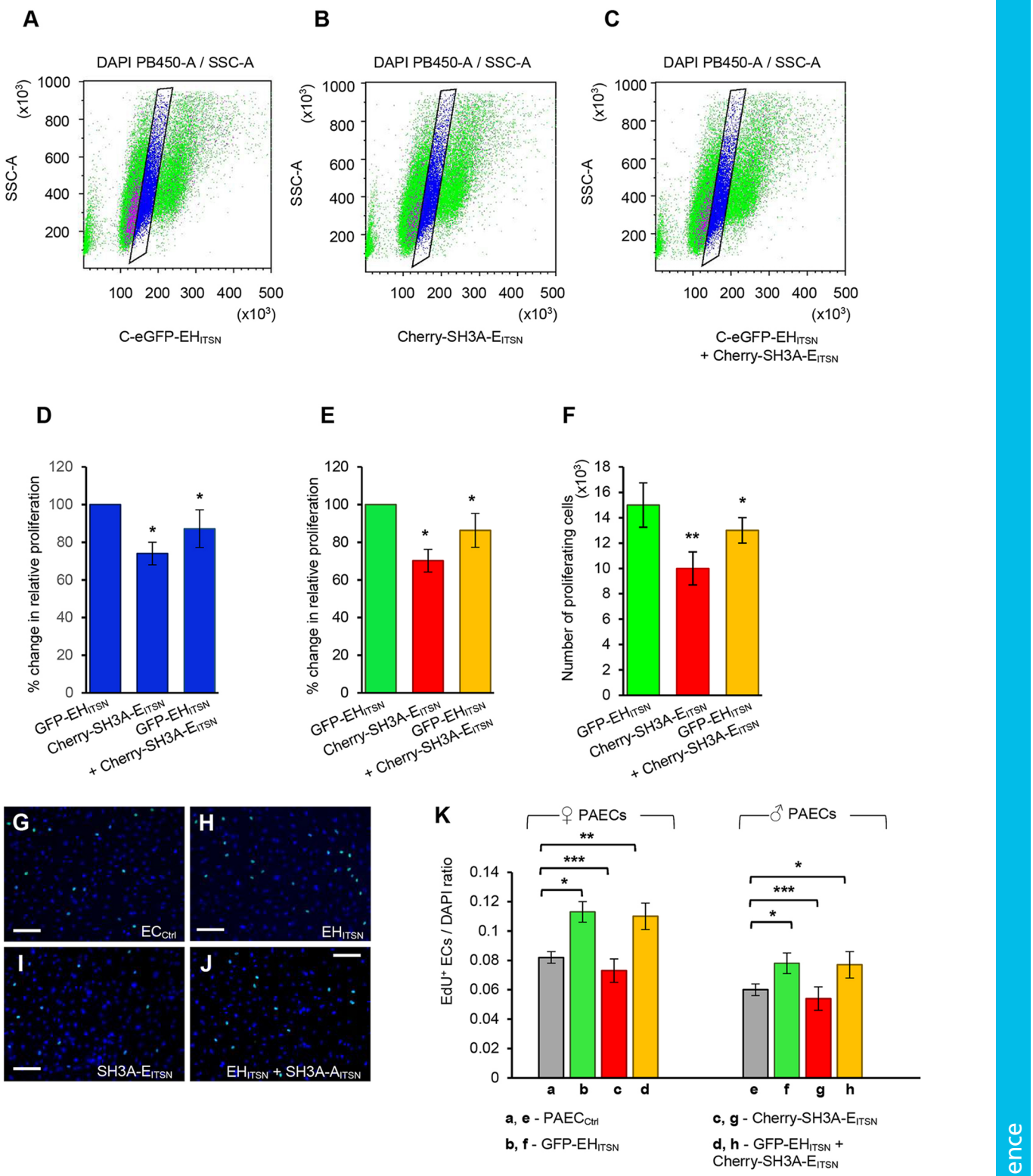

Fig. 3. PAECs show gender differences in the proliferative response to EH_{ITSN} expression. (A–C) Representative flow cytometry dot plots showing DAPI staining of the indicated transfected PAEC cell lines. Populations of proliferative PAECs in the S phase of the cell cycle are highlighted (boxed regions). (D) Mean±s.d. proliferation of PAECs transfected with mCherry-SH3A–E_{ITSN} or GFP-EH_{ITSN} and mCherry-SH3A–E_{ITSN}, relative to PAECs transfected with GFP-EH_{ITSN}. Data includes the entire mixed population of expressing and non-expressing cells. *P<0.05. (E) Mean±s.d. proliferation of transfected PAECs, as in D, but reporting data from cells expressing the relevant fluorescent tags. Gates used to define GFP- and mCherry-expressing cells were drawn based on untransfected control populations. At least 50,000 cells collected for each sample were analyzed. n=3. *P<0.05. (F) The number of proliferating cells, 48 h post-transfection, as indicated. Transfected cell lines were compared to untransfected controls; *P<0.05, **P<0.01. (G–J) Control PAECs ($PAEC_{Ctrl}$) and PAECs transfected with myc-EH_{ITSN}, FLAG-SH3A–E_{ITSN} or myc-EH_{ITSN} and FLAG-SH3A–E_{ITSN} were subjected to a Click-iT EdU Alexa Fluor proliferation assay followed by DAPI staining. Scale bar: 200 µm. (K) The ratio of EdU-positive to DAPI-stained transiently transfected female and male PAECs was used to estimate the proliferative rate of PAECs. Fifty high power fields of view were used for cell counting. Results are the mean±s.d. of three different experiments. *P<0.05; **P<0.01; ***P<0.001.

Journal of Cell Science (2020) 133, jcs237776. doi:10.1242/jcs.237776

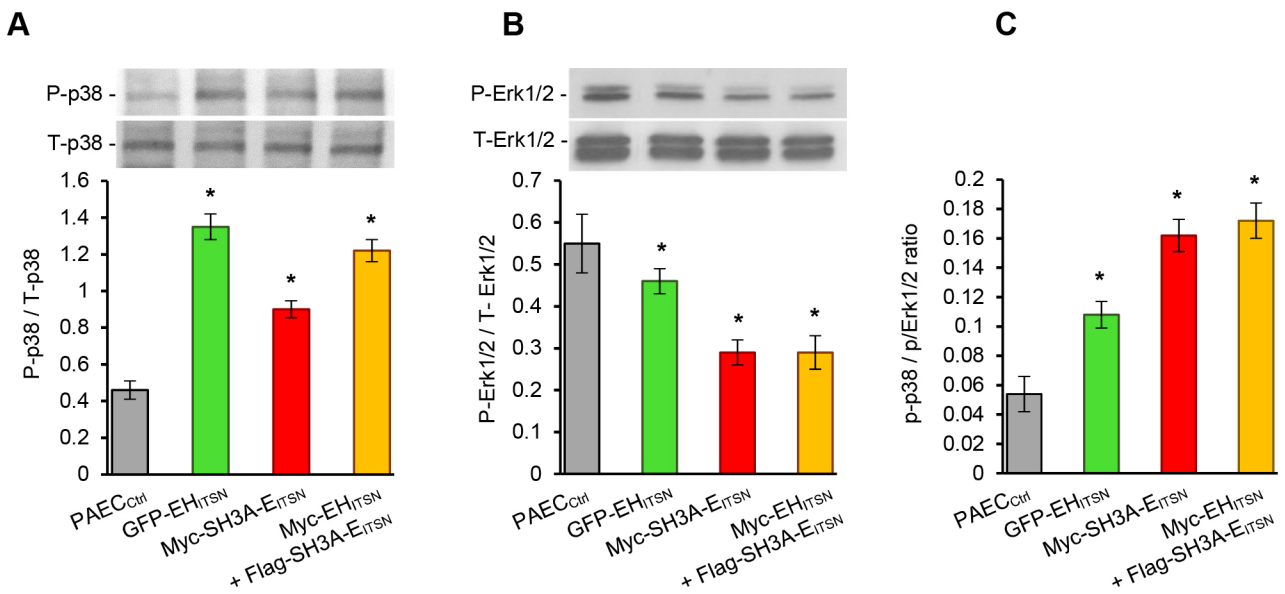

Fig. 4. Concurrent expression of EH_{ITSN} and SH3A–E_{ITSN} alters the ratio of p38 and ERK1/2 activity. (A,B) Lysates (70 µg total protein/well) of $PAEC_{Ctrl}$ donors and female PAECs transfected with myc-EH_{ITSN}, FLAG-SH3A–E_{ITSN} or myc-EH_{ITSN} and FLAG-SH3A–E_{ITSN} were subjected to western blotting using specific phospho- and total kinase antibodies, as indicated. Quantifications and representative blots are shown. *P<0.05 versus $PAEC_{Ctrl}$. (C) The ratio of p38 to ERK1/2 activity in control and transfected PAECs, as above. *P<0.01 versus $PAEC_{Ctrl}$. The ratios of phosphorylated (P-kinase) to total (T-kinase) kinase and of P-p38 to P-ERK1/2 are shown as mean±s.d. of at least three independent experiments.

Concurrent expression of the two protein fragments increases expression and activity of the ELK1 transcription factor

Nuclear extracts prepared from female PAECs transfected as above, alongside control PAECs, were subjected to an ELK1 transcription factor activation assay, as used by Patel et al. (2013, 2017), to evaluate the effects of concurrent expression of the two fragments on ELK1 activity (Fig. 5A). The presence of SH3A–E_{ITSN} did not cause significant changes in ELK1 activation; however, the values recorded in the assay also indicate that it does not prevent the endothelial pro-proliferative response to EH_{ITSN} expression. As our studies suggested that cultured human PAECs may show sex dimorphism in their proliferative response to the expression of ITSN fragments, we also evaluated the expression of ELK1, a transcription factor encoded on the X chromosome (chrX:47635519–47650604). Aliquots of nuclear extracts prepared from myc-EH_{ITSN}-transfected PAECs of male and female donors were subjected to western blotting using an ELK1 antibody (Fig. 5B). The expression of myc-EH_{ITSN} triggered an increase in ELK1 protein expression in female PAECs that was 35% greater than that triggered in male PAECs. When reverse transcription quantitative PCR (RT-qPCR) was used to determine the expression of *ELK1* mRNA, EH_{ITSN}-transfected female PAECs showed a greater than 3-fold increase in *ELK1* mRNA levels relative to the levels in female $PAEC_{Ctrl}$ (Fig. 5C).

EH_{ITSN} upregulates the expression of lncRNA *Xist* and increases proliferation of PAECs

Given the increased proliferation of female PAECs compared to the proliferation of male PAECs in response to EH_{ITSN} expression, and based on previous reports suggesting a critical role of lncRNA *Xist* upregulation in cell proliferation and in the molecular mechanisms of sex-biased diseases (Shenoda et al., 2018; Xu et al., 2017; Schurz et al., 2019), we performed an RT-qPCR to determine whether there is a correlation between expression of the *Xist* RNA gene and of the EH_{ITSN} protein fragment. Fig. 6A shows the relative expression of *Xist* RNA in non-transfected male and female control PAECs, confirming that the expression of *Xist* is significantly increased in female cells compared to the males. We then performed RT-qPCR on EH_{ITSN}-transfected male and female PAECs. Expression of EH_{ITSN} led to a significant upregulation of *Xist* expression, above basal levels, in both female and male PAECs, compared to the expression in control cells (Fig. 6A).

To further demonstrate that EH_{ITSN} induces *Xist* upregulation, female EH_{ITSN}-transfected PAECs were treated for 1 h at 37°C with 12.5 µM penetratin–NPF (PenNPF), an EH_{ITSN} inhibitory peptide [containing the NPF motif (Asn-Pro-Phe), which is the essential target of EH domains (de Beer et al., 1998)], or four different control peptides [p1, PenAAA (where the NPF motif was substituted with AAA); p2, penetratin sequence alone; p3, NPF (the NPF motif and residues vital for binding) and p4, a peptide consisting of the Pen sequence and a scrambled NPF sequence]. RT-qPCR revealed that exposure of EH_{ITSN}-transfected PAECs to the EH-inhibitory PenNPF peptide decreased *Xist* expression by 30%, whereas none of the control peptides affected *Xist* expression (Fig. 6B). When the effects of PenNPF treatment and subsequent *Xist* downregulation on cell proliferation were tested, EH_{ITSN}-transfected PAECs showed less proliferation by comparison to the proliferation of transfected PAECs with no peptide exposure, as indicated by a 3-(4,5-Dimethylthiazol-2-yl)-2,5-diphenyltetrazolium bromide (MTT) assay (Fig. 6C). The OD_{595} values of all wells containing EH_{ITSN}-transfected cells exposed to PenNPF–FITC were similar to those of wells containing $PAEC_{Ctrl}$ cells. The number of EH_{ITSN}-transfected cells in wells receiving PenNPF–FITC treatment was more than 35% lower than the number of EH_{ITSN}-transfected cells in wells not exposed to the PenNPF–FITC peptide (Fig. 6D). Exposure of EH_{ITSN}-treated PAECs to control peptides did not inhibit cell proliferation (Fig. 6D). However, a small inhibition with no statistical significance was caused by NPF treatment (Fig. 6D, p3), most likely due to the size (~1 kDa) and polar/non-polar amino acid content of the peptide conferring a low ability to penetrate cell membranes (Milletti, 2012). Fluorescence imaging of PAECs exposed to PenNPF–FITC indicated efficient peptide internalization

Journal of Cell Science (2020) 133, jcs237776. doi:10.1242/jcs.237776

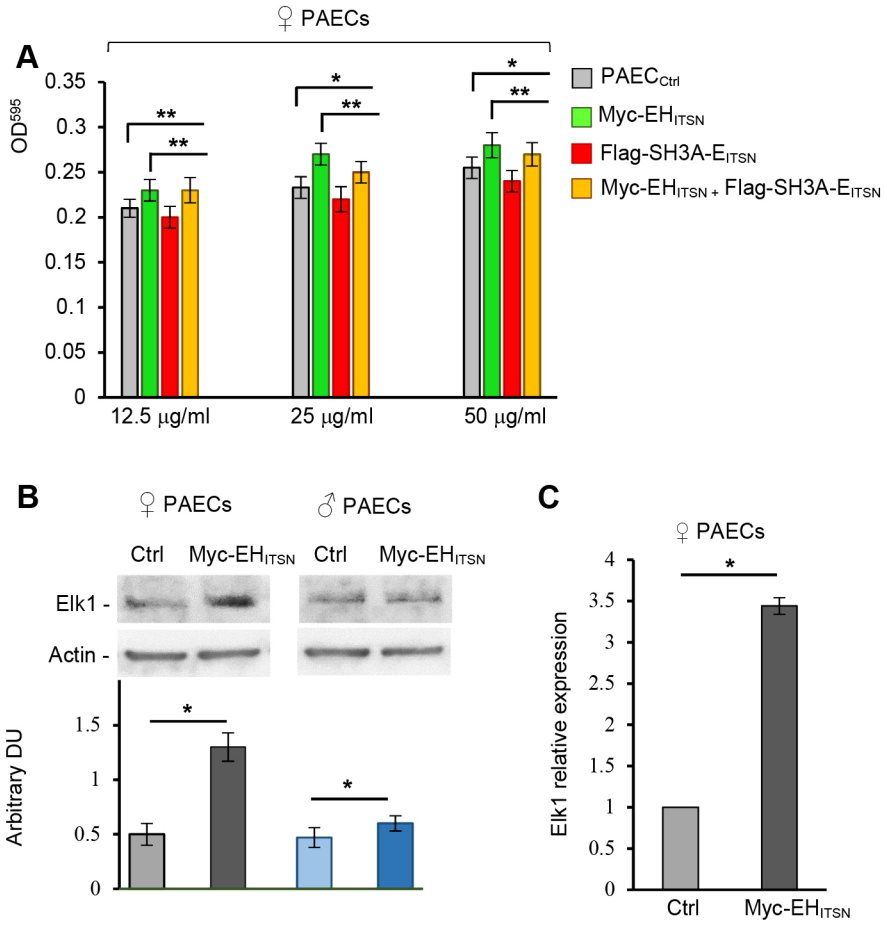

Fig. 5. Concurrent expression of EH_{ITSN} and SH3A–E_{ITSN} protein fragments increases the activity and expression of the ELK1 transcription factor. (A) Nuclear extracts (three different concentrations) prepared from control, EH_{ITSN}-, SH3A–E_{ITSN}- and EH_{ITSN} and SH3A–E_{ITSN}-transfected female PAECs were assayed for ELK1 activity using an ELISA kit designed to detect active ELK1. **P*<0.05, ***P*<0.01 versus $PAEC_{Ctrl}$ or EH_{ITSN}-transfected PAECs, as indicated. Data are mean±s.d. of three independent experiments performed in triplicate. (B) Nuclear extracts prepared from control (Ctrl) and EH_{ITSN}-transfected male and female PAECs, as indicated, were subjected to western blotting using a specific ELK1 antibody. Actin shown as a loading control. For purposes of comparison, detection of ELK1 immunoreactivity was performed using the same ELK1 and reporter antibody concentration and ECL exposure. Representative blots and a densitometric analysis of ELK1 immunoreactivity are shown, expressed as the ratio of ELK1 to actin signal. **P*<0.05. (C) RT-qPCR analysis of *ELK1* mRNA expression in EH_{ITSN}-transfected female and male PAECs. **P*<0.05 versus control female PAECs. Data are mean±s.d. of three independent experiments.

(Fig. 6E), while a PenNPF–FITC overlay approach, as described by Knezevic et al. (2011), confirmed direct interaction between the NPF motif and the EH_{ITSN} protein fragment (Fig. 6F). Although the increase in *Xist* expression was less dramatic in male EH_{ITSN}-transfected PAECs compared to that in female cells (Fig. 6A), this increase is consistent with the more modest increase in cell proliferation observed for these cells (Fig. 3K).

To further investigate the effects of the *Xist* lncRNA on proliferation of female PAECs, *Xist* expression was downregulated using an siRNA approach, specifically targeting *Xist* (siRNA XIST Smart*POOL*) (Fig. 6G). RT-qPCR revealed downregulation of *Xist* expression in siRNA-treated cells compared to expression levels in untreated PAECs or cells treated with control (scrambled) siRNAs. All four siRNA sequences against *Xist* downregulated *Xist* efficiently, with sequence 3 being the most efficient. We thereby chose sequence 3 for use in subsequent experiments. Given the significant upregulation of *Xist* in female EH_{ITSN}-transfected PAECs (Fig. 6A), we also investigated the involvement of *Xist* in the enhanced proliferative response of these female cells to EH_{ITSN} expression. Knockdown of *Xist* impaired proliferation of female PAECs by 50% compared to proliferation of untreated PAECs or cells treated with the control siRNA sequence (Fig. 6H).

PAECs from female idiopathic PAH patients show increased *Xist* expression and transcriptional activity

To validate these observations in a physiologically relevant disease context, we used PAECs isolated from idiopathic PAH male and female patients (Table S2). PAECs isolated from non-disease subjects (ND-Ctrl) of both genders were used for comparison. We first examined the expression of the lncRNA *Xist* by RT-qPCR and found that expression was higher in female $PAEC_{PAH}$ than female $PAEC_{ND\text{-}Ctrl}$ cells (Fig. 7A). As expected, *Xist* expression was significantly lower in male cell lines than in female cell lines, with expression values extending over a wide range (Fig. 7B). We also used a luciferase-based assay to investigate the transcriptional activity of *Xist*. $PAEC_{ND\text{-}Ctrl}$ and $PAEC_{PAH}$ of male and female patients were co-transfected with an *Xist* firefly luciferase reporter vector and a control Renilla luciferase construct. The relative luciferase activity, calculated based on the ratio of firefly luciferase to Renilla luciferase fluorescence, indicated that *Xist* transcriptional activity in $PAEC_{PAH}$ cells is higher compared to the activity in $PAEC_{ND\text{-}Ctrl}$ cells, by 2.3-fold in cells from female patients and 1.5-fold in cells from male patients (Fig. 7C).

As *ELK1* is an X-linked gene implicated in the pathogenesis of plexiform PAH, we also examined *ELK1* expression in $PAEC_{PAH}$ by RT-qPCR. *ELK1* expression was upregulated in female $PAEC_{PAH}$ (Fig. 7D), whereas no change in *ELK1* expression was detected in the male $PAEC_{PAH}$ compared to $PAEC_{ND\text{-}Ctrl}$. Of note, the values for *ELK1* expression in female PAECs extend over a wider range compared to that in male cells, which is likely consistent with the regulation of its expression by the abnormally expressed *Xist*.

As recent studies indicated that KLF2, a relevant transcription factor for PAH pathogenesis due to its role in EC proliferation and antiangiogenic effects (Atkins and Jain, 2007; Fang et al., 2016) is a *Xist* target, we next examined the expression of *KLF2* in male and female PAECs of ND-Ctrl and PAH patients. RT-qPCR analyses revealed that *KLF2* expression was downregulated in female

Journal of Cell Science (2020) 133, jcs237776. doi:10.1242/jcs.237776

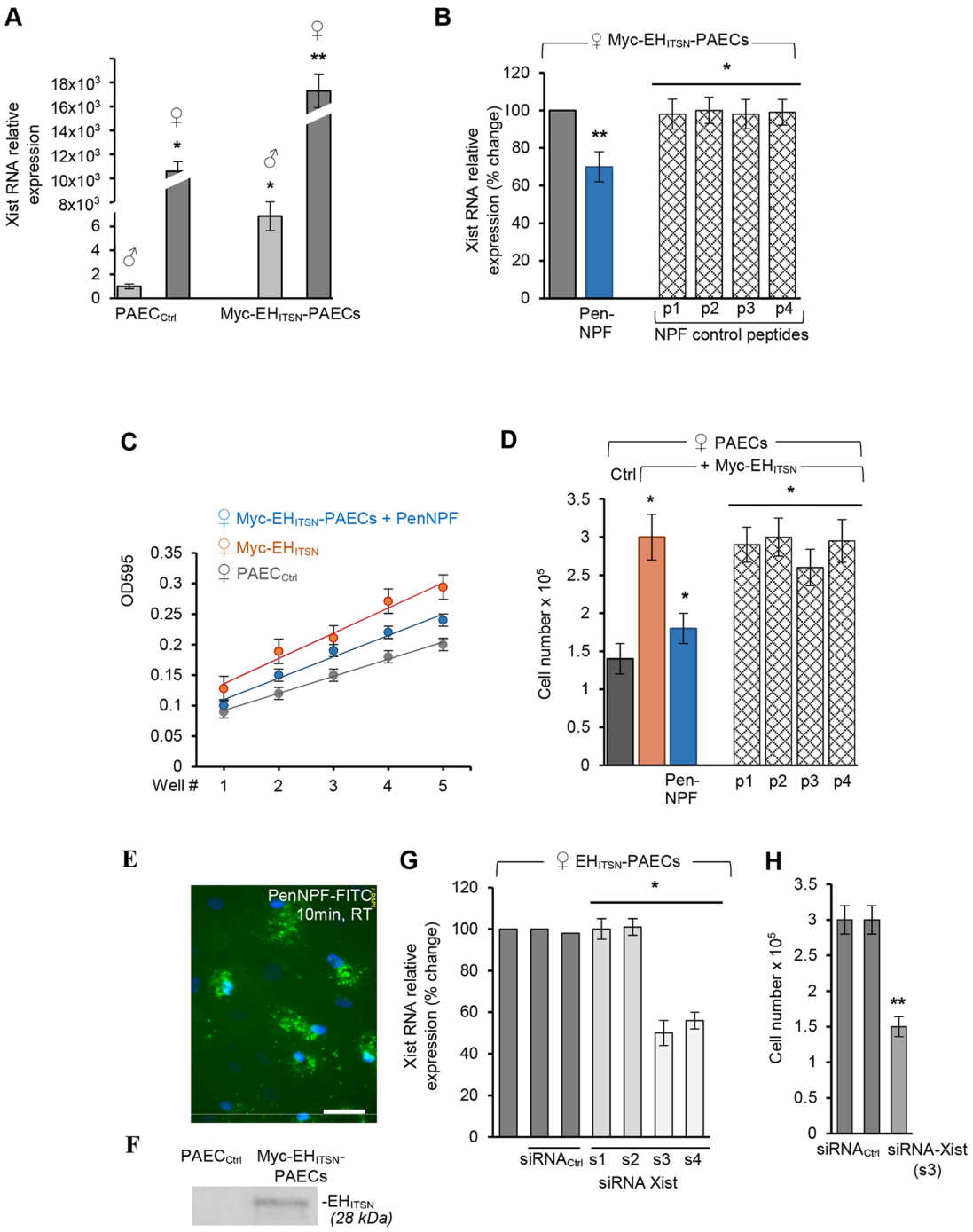

Fig. 6. EH$_{ITSN}$ upregulates the lncRNA *Xist* and increases PAEC proliferation. (A) Relative expression of lncRNA *Xist* in male and female non-transfected PAEC$_{Ctrl}$ and EH$_{ITSN}$-transfected PAECs. (B) Relative expression of *Xist* in female EH$_{ITSN}$-transfected PAECs with or without 12.5 µm PenNPF or control peptide treatment for 12 h, as indicated. p1, Pen-AAA (NPF substituted with the AAA sequence); p2, Pen alone; p3, NPF (NPF and the vital residues for binding); p4, Pen (scrambled) NPF peptide. Data are normalized to the untreated control. (C) MTT assay applied to female PAEC$_{Ctrl}$ and EH$_{ITSN}$-transfected PAECs with and without 12.5 µM PenNPF peptide. Data represent dilution series conducted in triplicate for each experimental condition. (D) Quantification of PAEC proliferation. Growth curve data was used to relate the OD$_{595}$ values shown in C to cell number. Graph shows cell numbers for female PAEC$_{Ctrl}$, EH$_{ITSN}$-transfected PAECs, and EH$_{ITSN}$-transfected PAECs exposed to PenNPF, Pen-AAA (p1), Pen alone (p2), NPF alone (p3) and scrambled peptide (p4). Data in A–D are mean±s.d. of three independent triplicate experiments. *P<0.05, **P<0.01 versus male PAEC$_{Ctrl}$ in A, versus female EH$_{ITSN}$-transfected PAECs in B and versus female PAEC$_{Ctrl}$ in D. (E) Fluorescent imaging of PAECs exposed to 12.5 µM PenNPF–FITC, for 10 min at room temperature (RT). Scale bar: 50 µm. (F) PAEC$_{Ctrl}$ and EH$_{ITSN}$-transfected PAEC lysates (70 µg total protein) resolved using SDS–PAGE and transferred to nitrocellulose membranes were overlaid with 5 µM PenNPF–FITC peptide per ml. The bound peptide was detected using a FITC antibody. Blot is representative of n=3 experiments. (G) Relative expression levels of *Xist* in female EH$_{ITSN}$-transfected PAECs assayed 72 h after transfection with two siRNA$_{Ctrl}$ sequences or with the specific Smart*POOL* reagent (siRNA *Xist*, sequences s1–s4). (H) Quantification of cell number of female EH$_{ITSN}$-transfected PAECs, 72 h post-*Xist* siRNA transfection using the Xist siRNA sequence s3. Two scrambled siRNA sequences served as controls. Data in G and H are mean±s.d. of three independent experiments. *P<0.05 and **P<0.01 versus female EH$_{ITSN}$-transfected PAECs in G and versus control siRNA-treated female EH$_{ITSN}$-transfected PAECs in H.

Journal of Cell Science (2020) 133, jcs237776. doi:10.1242/jcs.237776

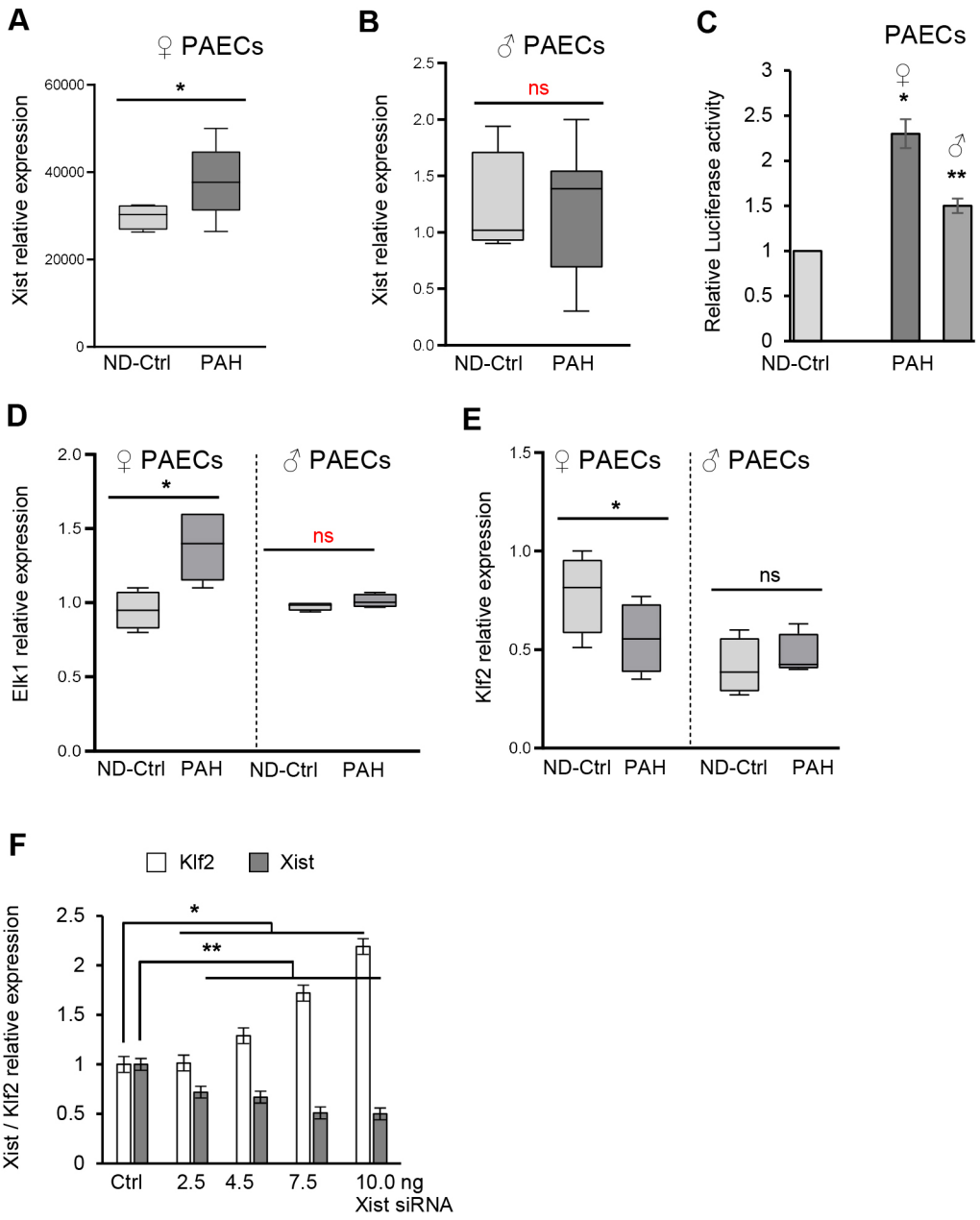

Fig. 7. lncRNA *Xist* is upregulated in female $PAEC_{PAH}$ and regulates the expression of ELK1 and KLF2 transcription factors. (A,B) The relative expression of *Xist* in PAECs isolated from female and male ND-Ctrl and idiopathic PAH patients, as determined by RT-qPCR. **P*<0.05; ns, not significant. (C) Luciferase activity in ND-Ctrl PAECs and PAECs of male and female PAH patients. Data are mean±s.d. of triplicate transfections representing at least three experiments. **P*<0.05, ***P*<0.01. (D,E) The relative expression of *ELK1* and *KLF2*, respectively, in PAECs of female and male ND-Ctrl and PAH patients, as determined by RT-qPCR. **P*<0.05; ns, not significant. (F) RT-qPCR analysis showing that *Xist* knockdown in EH_{ITSN}-transfected female PAECs through siRNA treatment (sequence s3) restores *KLF2* expression. Data shown are mean±s.d. **P*<0.05; ***P*<0.01. G*APDH* expression was used for normalization for all RT-qPCR analyses, and all experiments were performed in triplicate. In A, B, D and E, *n*=5 PAEC lines per experimental condition. Whiskers indicate the range, boxes indicate the 25th to 75th percentile and horizontal bars indicate median values.

$PAEC_{PAH}$ compared to the female baseline healthy state, but no significant difference in expression was detected between male $PAEC_{PAH}$ and the male baseline healthy state (Fig. 7E). Interestingly, *KLF2* gene expression was different between sexes even at the baseline healthy state (Fig. 7E), suggesting that *Xist* upregulation has a significant effect on *KLF2* expression in female PAECs. Thus, the extent of *KLF2* expression downregulation between female PAH and female control cells underlies the functional significance of *KLF2* repression in PAH. Moreover, siRNA-mediated *Xist* knockdown, an experimental manipulation that decreases EC proliferation as shown above (Fig. 6H), augmented *KLF2* expression (Fig. 7F). Based on these findings we conclude that *Xist* upregulation may account for the gender bias in PAH on two accounts: first, by causing aberrant expression of the gene encoding the ELK1 transcription factor, an X-linked gene involved in PAH pathogenesis, and second, through regulation of its downstream target, *KLF2*.

The PenNPF peptide, a specific inhibitor of EH_{ITSN}, inhibits activation of p38–ELK1–c-Fos signaling

As EH_{ITSN} triggers proliferation of PAECs via the p38–ELK1–c-Fos signaling pathway, we investigated if the PenNPF peptide, which decreases *Xist* lncRNA expression, also inhibits this signaling pathway. Western blotting using antibodies to recognize phosphorylated p38 was conducted on lysates of $PAEC_{Ctrl}$, untreated EH_{ITSN}-transfected PAECs and EH_{ITSN}-transfected PAECs treated with PenNPF and control peptides. Densitometric analyses showed a 70% decrease in p38 activation in transfected cells treated with the PenNPF peptide compared to p38 activation in untreated transfected cells (Fig. 8A). EH_{ITSN}-expressing PAECs treated with control peptides did not show significant changes in p38 activation. Nuclear extracts from EH_{ITSN}-transfected PAECs treated with PenNPF showed a 55% decrease in ELK1 activation compared to untreated transfected PAECs (Fig. 8B). Similar results were also obtained for c-Fos expression. Treatment with the

Journal of Cell Science (2020) 133, jcs237776. doi:10.1242/jcs.237776

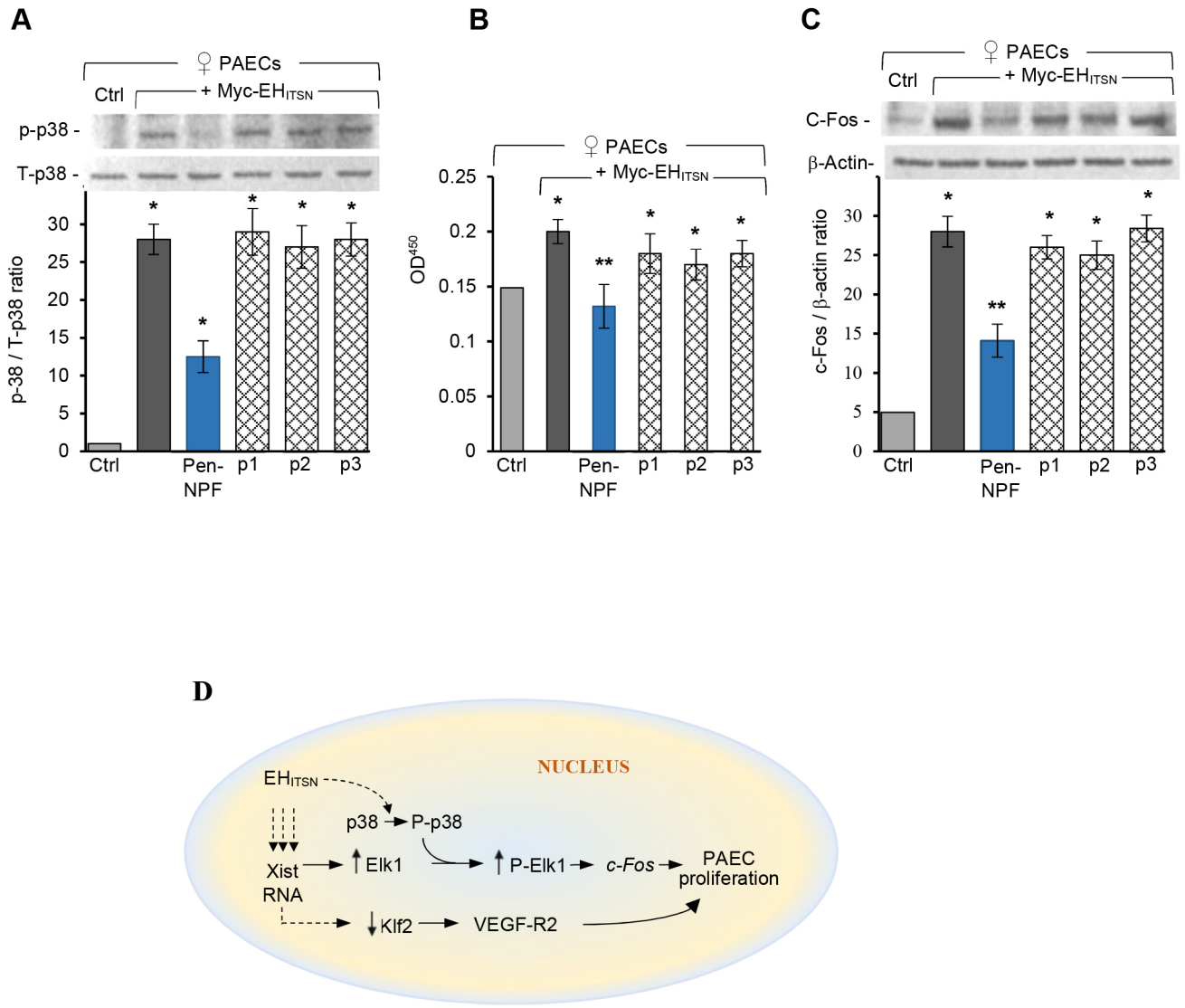

Fig. 8. The PenNPF peptide decreases activation of p38–ELK1–c-Fos signaling. (A) Lysates from female $PAEC_{Ctrl}$ and EH_{ITSN}-transfected PAECs, untreated or treated with PenNPF and control peptides, were analyzed for p38 phosphorylation. Data were normalized to total kinase signal. Mean±s.d. densitometric values are shown with representative blot images. *n*=3 independent experiments. **P*<0.001 versus $PAEC_{Ctrl}$ (Ctrl), apart from Pen-NPF sample where **P*<0.001 versus untreated transfected cells. (B) Nuclear extracts prepared from female $PAEC_{Ctrl}$ and EH_{ITSN}-transfected PAECs, untreated or treated with peptides, were assayed for ELK1 activity. Data are mean±s.d. of *n*=3 independent experiments performed in triplicate. **P*<0.05 versus $PAEC_{Ctrl}$ (Ctrl); ***P*<0.01 compared to untreated transfected PAECs. (C) Western blotting of nuclear extracts (45 µg protein/lane) from female $PAEC_{Ctrl}$ and EH_{ITSN}-transfected PAECs, untreated or treated with peptides using a c-Fos antibody. Data were normalized to β-actin signal and represent mean±s.d. for *n*=3 different experiments. **P*<0.05 versus $PAEC_{Ctrl}$ (Ctrl), ***P*<0.01 compared to untreated transfected female PAECs. (D) Diagram of the proposed EH_{ITSN}- and *Xist*-mediated molecular mechanism to explain sexual dimorphism in the proliferative response of PAECs. EH_{ITSN} translocates to the nucleus to modulate the expression of *Xist* and activate p38 kinase. The p38 kinase directly phosphorylates and interacts with the transcription factor ELK1; p38 kinase activity is necessary for the recruitment of ELK1 to the *c-Fos* promoter (Ferreiro et al., 2010). Moreover, increased *Xist* expression upregulates expression of the X-linked gene *ELK1* and downregulates KLF2, an *Xist* downstream target, leading to increased expression of VEGF Receptor 2 (VEGF-R2) and increased proliferation of PAECs. Thus, *Xist* upregulation could be an important factor to explain sexual dimorphism in the proliferative response of PAECs and the imbalanced sex ratio of PAH.

PenNPF peptide decreased c-Fos expression in EH_{ITSN}-transfected cells by 53% compared to expression in untreated EH_{ITSN}-transfected cells and transfected PAECs treated with control peptides (Fig. 8C).

Based on these data, we propose a model in which EH_{ITSN} translocated into the nucleus may have a dual function, to modulate *Xist* expression and to activate p38 kinase (Fig. 8D). *Xist* upregulation may control expression of ELK1, a transcription factor encoded by a gene located on chromosome X that is an important link between hypoxia, *c-Fos* and c-Fos target genes. Xist upregulation could also affect the expression of KLF2, a transcription factor with potent antiangiogenic effects and a known *Xist* target (Fang et al., 2016; Yu et al., 2015; Carman et al., 2019). These molecular alterations may explain the sexual dimorphism in the proliferative potential of PAECs and the increased susceptibility of women to PAH.

DISCUSSION

Inflammatory processes are recognized as a major pathogenic component of pulmonary vascular remodeling in PAH (Hassoun et al., 2009). Increased pulmonary expression of different cytokines and chemokines, the identification of perivascular cell infiltrates composed of macrophages, T cells and B cells in plexiform lesions

Journal of Cell Science (2020) 133, jcs237776. doi:10.1242/jcs.237776

in the lungs of PAH patients and correlation of perivascular inflammation with intima and media remodeling support this inflammatory component in PAH (Dorfmuller et al., 2003; Sanchez et al., 2007; Tuder et al., 1994; Stacher et al., 2012). Previous studies using human lung PAH specimens have shown that GrB immunoreactivity is associated with plexiform lesions of small pulmonary arteries (Patel et al., 2017). These observations are consistent with the fact that during PAH progression, when T-cell inflammation is persistent, GrB cleaves ITSN, a prominent protein of the lung tissue with a well-conserved GrB cleavage site (Patel et al., 2013; Loeb et al., 2006), and generates two cleavage products, with the N-terminal fragment (EH_{ITSN}) possessing EC proliferative potential. The lung tissue of PAH animal models and human specimens, as well as PAECs of PAH patients, express the EH_{ITSN} cleavage fragment, an important modifier of endocytic activity in PAECs (Patel et al., 2013). Our recent studies show that EH_{ITSN} expression alters the subcellular localization of EH domain-binding protein 1 and the organization of cortical actin, resulting in increased trafficking through alternative endocytic structures (Predescu et al., 2012). Moreover, transient expression of the SH3A–E_{ITSN} fragment in PAECs specifically inhibits caveolae-mediated endocytosis by sequestering dynamin-2, the membrane fission GTPase, in the cytosol away from the neck region of endocytic vesicles (Predescu et al., 2003). However, when the EH_{ITSN} and SH3A–E_{ITSN} fragments are concurrently expressed it appears that the ability of EH_{ITSN} to shift the physiological vesicular (caveolae-mediated) transport towards alternative endocytic pathways (Predescu et al., 2012) overcomes the endocytic deficiency generated by SH3A–E_{ITSN} expression, and EC endocytic activity stays at the basal level. Thus, despite the dominant-negative effects of SH3A–E_{ITSN} expression, EH_{ITSN} still contributes to the endocytic activity, proliferation and overgrowth of dysfunctional PAECs, and hence, to the development and maintenance of the dysfunctional $PAEC_{PAH}$ phenotype and to progression of the disease.

Besides being the molecular backbone of membrane trafficking, endocytic scaffold proteins can affect cellular proliferation and signaling at both the nuclear and cytoplasmic level. Similar to other endocytic proteins, ITSN undergoes nucleo-cytoplasmic trafficking that may allow it to perform specialized tasks in the nucleus, such as regulation of cellular proliferation and transcription (Alvisi et al., 2018). Previous studies indicated that the src homology-3 (SH3) domain and the coiled-coil domain of ITSN mediate an interaction with importin and thus, ITSN is capable of nucleo-cytoplasmic shuttling in a chromosome region maintenance 1-dependent manner (Alvisi et al., 2018). In addition to the roles of the coiled-coil and SH3 domains, the N-terminal EH motif(s) may also be responsible for the localization of endocytic proteins, including ITSN, in the nucleus (Predescu et al., 2018; Borlido et al., 2009). Ectopically expressed myc-EH_{ITSN} was found to be predominantly present in the cytosol; however, a hefty fraction showed nuclear localization. We have shown that EH_{ITSN} expression triggers persistent and specific p38 phosphorylation (Patel et al., 2013). p38 kinase has been reported to regulate gene expression through direct phosphorylation and interaction with transcription factors responsible for activation of target genes. p38 activity is necessary for the recruitment of ELK1 to the *c-Fos* promoter and for *c-Fos* transcriptional upregulation (Ferreiro et al., 2010). Thus, prolonged expression of the EH_{ITSN} fragment triggers p38-dependent signaling, which results in activation of the transcription factor ELK1 and the immediate-early response gene *c-Fos*, and EC proliferation. Conversely, chemical inhibition of p38 kinase activity interferes with proliferation of EH_{ITSN}-expressing PAECs (Patel et al., 2017, 2013).

The C-terminal cleavage product of ITSN comprises a coiled-coil region and five consecutive SH3 domains. Expression of the full SH3A–E_{ITSN} sequence, or truncated versions, in different cell types (including ECs) indicated that this motif sequesters SOS1, a Ras-specific guanine-nucleotide-exchange factor, resulting in a dominant-negative effect on Ras–ERK1/2 signaling (Tong et al., 2000a; Bardita et al., 2013). The molecular mechanisms involved in balancing the proliferative and apoptotic signaling controlled by the two cleavage products, and the physiological and pathological implications, are complex and not fully understood. This study provides *in vitro* evidence that, when concurrently expressed, the two protein fragments of ITSN increased not only p38 activation, an event associated with proliferation of PAECs and formation of plexiform lesions (Patel et al., 2017), but also the ratio of p38 to ERK1/2 activity. It seems that SH3A–E_{ITSN} cooperates with EH_{ITSN} in activation of the p38–ELK1 pathway to support pathological excessive proliferation of PAECs. Given the proliferative effects of concurrent expression of EH_{ITSN} and SH3A–E_{ITSN} detected in our cellular context, the possibility that SH3A–E_{ITSN} undergoes nucleo-cytoplasmic trafficking and is involved in regulation of EC proliferation and perhaps transcriptional processes cannot be ruled out.

Moreover, concurrent expression of the two protein fragments augmented p38 and ELK1 activation and the ratio of p38 to ERK1/2 activity, with female cells being more responsive than the male cells. Dysregulated MAPK signaling is observed in various experimental models of PAH (Awad et al., 2016). Although the relative significance of any given signaling pathway studied thus far seems to be influenced by the specific animal strain, stimulus, age, sex, environment and cell type used, the activation of p38 appears to be a characteristic of animal models of PAH that develop plexiform lesions (Carman et al., 2019). This observation suggests that the formation of plexiform lesions in different systems may share a common pathophysiological mechanism that converges on p38 activation (Carman et al., 2019).

Accumulating evidence indicates that lncRNA regulation plays key roles in the development and progression of many human diseases (Yang et al., 2018). lncRNAs are involved in many aspects of gene regulation, including epigenetic regulation, imprinting, trafficking between the nucleus and cytoplasm, transcription and mRNA splicing (Yang et al., 2018). Abnormal levels of the lncRNA *Xist* interfere with the expression profiles of X-linked genes and have been linked to tumorigenesis, cell cycle regulation, apoptosis, and cell proliferation. Recent studies demonstrated that *Xist* is abnormally expressed in several cancers, with a negative relation to clinical outcome, and that abnormal expression of *Xist* may partially contribute to sex biases in cancer (Yang et al., 2018). Altered expression of X-linked genes is observed in female-biased autoimmune disorders and mouse models of autoimmunity (Libert et al., 2010). Chromosome X has the greatest density of immunity-related genes, and thus females, with two X chromosomes, have an immunological advantage over males (XY). The strong female-specific immune response is not always beneficial and can result in autoimmunity (Wang et al., 2016). Thus, aberrant expression of the lncRNA *Xist*, although essential for X-chromosome inactivation and dosage compensation of X-linked gene expression (Yang et al., 2018), might also affect the expression of genes carried on human and mouse chromosome X that are documented to be involved in PAH pathogenesis (Table S3) including apelin (Brash et al., 2018; Yang et al., 2017, 2019), tissue inhibitor of metalloproteinase-1 (Tiede et al., 2016; Chelladurai et al., 2012; Wang et al., 2015), histone deacetylase 6 (Boucherat

Journal of Cell Science (2020) 133, jcs237776. doi:10.1242/jcs.237776

et al., 2017), angiotensin-converting enzyme 2 (Hemnes et al., 2018; Li et al., 2013), filamin (Huang et al., 2018; Hirashiki et al., 2017), O-linked beta-N-acetyl-glucosamine (Barnes et al., 2015), host cell factor-1 (Barnes et al., 2015), androgen receptor (Elinoff et al., 2013), nicotinamide adenine dinucleotide phosphate oxidase (Ghouleh et al., 2017; Hood et al., 2016) and *ELK1* (Patel et al., 2017). Dysregulation of *Xist* can result in genes escaping inactivation or reactivation in female cells (Vacca et al., 2016). Our results revealed that in female PAECs, *Xist* was upregulated above basal levels in response to EH_{ITSN} expression, an event that caused an increase in their proliferation rate. In addition, female PAECs showed increased expression of the X-linked gene *ELK1*, 3.4-fold greater than expression in male PAECs,

Thus, similar to other types of human ECs, such as pulmonary microvascular ECs (Addis et al., 2014) and umbilical ECs (Zhang et al., 2018), PAECs display sexual dimorphism that affects their response to EH_{ITSN} expression. Inhibition of EH_{ITSN} using a highly specific EH-inhibitory peptide abolished both the increase in *Xist* expression and PAEC proliferation. PAEC proliferation was also abolished by siRNA-mediated *Xist* knockdown. Altogether, these findings suggest a causal link between EH_{ITSN} expression, Xist upregulation, and PAEC proliferation.

The increased responsiveness of female cells to EH_{ITSN} expression was due to upregulation above basal levels of the lncRNA *Xist*, because downregulation of *Xist* gene expression using siRNA knockdown or treatment with a highly specific EH_{ITSN} inhibitory peptide decreased PAEC proliferation and activation of the p38–ELK1–c-Fos signaling pathway. Thus, *Xist* upregulation could explain the sexual dimorphism in the proliferative potential of PAECs and the increased susceptibility of women to PAH. Of particular interest is the finding that PAECs of female PAH patients, a physiologically relevant disease setting, recapitulated the *in vitro* results. The PAECs of female PAH patients showed upregulation of *Xist* expression above the baseline healthy state and increased *ELK1* expression, two molecular events that may account for the increase in their proliferation rate. In this study we also found that upregulation of *Xist* in PAECs of PAH female patients was associated with repression of KLF2 transcription factor expression. KLF2 deficiency has been implicated in PAH pathogenesis (Eichstaedt et al., 2017; Kim, 2014; Kim et al., 2015), but so far has not been related to gender differences. Previous reports indicated that in non-small cell lung cancer, *Xist* interacts with enhancer of zeste homolog 2, an RNA binding protein that is the catalytic subunit of the Polycomb Repressive Complex 2, to repress *KLF2* expression (Fang et al., 2016). Moreover, *Xist* can interact with miR-92a, a miRNA that targets KLF2 and that might also regulate KLF2-dependent genes (von Willebrand factor, Tie-2, FLK-1, VEGF-R2) important for regulation of endothelial functions (Wu et al., 2011; Yu et al., 2015).

As shown in Fig. 8, the mechanisms underlying the effects of *Xist* upregulation in response to EH_{ITSN} expression are complex and might involve multiple parts of the *Xist* regulatory network (i.e. all levels of gene regulation, including *cis*-regulatory elements, transcription factors, chromatin modifications and higher-order chromatin structure), as well as the targets of *Xist*, such as the X-linked PAH genes. Understanding the complex relationship between *Xist* and proliferation of PAECs remains challenging, and more work is needed to develop the use of *Xist* as a diagnostic and prognostic marker and a therapeutic target for the treatment of PAH in women. Though this is a robust study, we employed only five $PAEC_{PAH}$ cell lines. Owing to this relatively small sample size, the findings should be complemented by additional studies of PAECs and lung tissue of PAH patients in order to further elucidate the role of upregulation of Xist expression in PAH. Mechanistic studies on how the expression of X-linked genes and transcription factors involved in PAH can be influenced by changes in *Xist* expression levels are needed to validate our findings.

MATERIALS AND METHODS

Materials

Non-disease (control) human pulmonary artery endothelial cells (PAECs) from male and female donors, Endothelial Basal Medium (EBM-2), Medium 199 and EGM-2 Endothelial Growth SingleQuots Kit Supplement and Growth Factors were from Lonza (Walkersville, MD). X-tremeGENE HP DNA transfection reagent was from Roche Applied Science (Mannheim, Germany). EZ-Link Sulfo NHS-SS-Biotin, Click-iT EdU Alexa Fluor Cell Proliferation kit, ProLong Gold Antifade reagent with DAPI, NeutrAvidin-Dylight 594 conjugated, Foxp3 Staining Buffer set, DAPI Nucleic Acid Stain and NE-PER Nuclear and Cytoplasmic Extraction kit were from Thermo Fisher Scientific (Hanover Park, IL). MTT Cell Proliferation Assay kit was from ATCC (Manassas, VA). Streptavidin-HRP-conjugated was from EMD Millipore Corporation (Temecula, CA). Antibodies used were as follows: phospho-p38 mAb (T180/Y182; #4631S), p38 pAb (#9212S), phospho-ERK1/2 mAb (T282/Y284; #4370S), ERK1/2 pAb (#9102S), myc-tag mAb (#2276S), FLAG-tag mAb (#14793S) and c-Fos rabbit Ab (#2276) from Cell Signaling Technology (Beverly, MA); actin mAb (#sc-47778) and ITSN1 Ab (EH epitope; #ABN1378) from Sigma-Aldrich (St. Louis, MO); ELK1 pAb (#sc-355) and FITC Ab from Santa Cruz Biotechnology (Santa Cruz, CA); KLF2 Ab (#PA5-40591) from Thermo Fisher Scientific (Hanover Park, IL), HRP-conjugated reporter antibodies from Cappel, Organon Teknika (Durham, NC). Specific Xist siRNA SmartPOOL reagent and control (scrambled nucleotide) sequences were from Dharmacon (Lafayette, CO). The PenNPF and control peptides were synthesized by the Protein Core, University of Illinois at Chicago.

Cell culture and transfection

Male and female PAECs were grown as described by Patel et al. (2013). For transfection, EH_{ITSN} cDNA (encoding amino acids 3–271) was cloned into the pReceiver/Myc-M43 and CS-Z3999-M03/C-eGFP vectors while the SH3A–E_{ITSN} cDNA (encoding amino acids 744–1206) was cloned into the pReceiver/Flag-M12 and the pReceiver/Cherry-M55 vectors (GeneCopoeia, Rockville, MD). All transfections were performed using an optimized 3:1 (µl:µg) ratio of X-tremeGENE 9 DNA transfection reagent to DNA. For co-transfection experiments, PAECs were grown to 90% confluency and the transfection mixtures were added at the same time. Empty vector was used as control throughout.

Localization of GFP- and mCherry-tagged ITSN fragments in transfected PAECs was determined by imaging with excitation at 488 nm and emission at 500–550 nm for GFP, and excitation at 568 nm and emission at 580–700 nm for mCherry.

For siRNA transfection, the Xist Smart*POOL* Reagent, four sequences designed and synthesized by Dharmacon, were prepared as 50 µM stock solutions and stored at −80°C until use. PAECs grown in complete endothelial media (EBM-2 and Medium 199 supplemented with 20% fetal calf serum) at 37°C, in 60 mm Petri dishes, were transfected with lipoplexes as follows: 4 µg of siRNA was added to 396 µl of serum-free media mixed with 4.34 µl Dharmafect, as per the manufacturer's protocol. Cells were collected 72 h after transfection and analyzed by RT-qPCR for *Xist* expression.

Male and female idiopathic $PAEC_{PAH}$ and ND-Ctrl PAECs were from the Pulmonary Hypertension Breakthrough Initiative (PHBI) or kindly provided by Drs Serpil Erzurum and Suzy Comhair (Lerner Research Institute, Cleveland Clinic, Cleveland, OH) at passages 3–5. The PAECs were harvested and cultured as described in Comhair et al. (2012). The PAECs were de-identified in accordance with the Health Insurance Portability and Accountability Act and authenticated to confirm their endothelial identity. The studies were conducted in compliance with the PHBI guidelines, as per the MTA agreement. These studies did not meet the definition of human subject research (15090702-IRB02-CR04).

Journal of Cell Science (2020) 133, jcs237776. doi:10.1242/jcs.237776

Protein extraction, western blotting and immunoprecipitation

Human PAECs grown on Petri dishes were collected and solubilized in lysis buffer [20 mM Tris-HCl, pH 7.4, 150 mM NaCl, 0.3% SDS, 1% (w/v) Triton X-100, 1 mM Na_3VO_4, 1 mM PMSF, protease and phosphatase inhibitors (Sigma-Aldrich, St Louis, MO)] for 1 h at 4°C under gentle agitation. The resulting lysate was clarified by centrifugation in a Beckman Optima Max-XP ultracentrifuge, TLA-55 rotor at 45,000 rpm for 45 min at 4°C. Protein concentration was determined using the BCA method with a BSA standard. Cell lysates (70 µg total protein/lane), were subjected to SDS–PAGE on a 4–20% gel and transferred to nitrocellulose membranes, which were probed with antibodies for detection of phospho-p38 and total p38 (1:1000), phospho-ERK1/2 and total ERK1/2 (1:1000), myc-tag (1:500), FLAG-tag (1:500), c-Fos (1:100) and ELK1 (1:100). An antibody for detection of actin (1:2000) was used as a loading control. HRP-conjugated reporter antibodies were used at 1:1000 dilution. Western blots were visualized using ECL and HyBlot CL films. Representative HyBlot CL films were subjected to densitometry using ImageJ software (1.37v; NIH, MD). For immunoprecipitation, nuclear and cytosolic fractions (350 µg total protein) prepared from PAECs were pre-cleared with Protein A/G for 1 h at room temperature, followed by overnight incubation with 2 µg anti-myc antibody and 30 µl Protein A/G slurry at 4°C. Beads were extensively washed and the resulting immunoprecipitates were solubilized in electrophoresis sample buffer then analyzed by SDS–PAGE and western blotting, as above.

Biotin internalization assay

Transfected PAECs grown on plastic Petri dishes or glass coverslips were washed with ice-cold PBS and then incubated with 0.5 mg/ml cleavable biotin reagent as reported previously (Predescu et al., 2003). Biotinylated cell surface proteins were internalized for 20 min at 37°C. Biotinylated proteins still at the cell surface after 20 min were reduced with glutathione and the cells were further processed for morphological analyses or lysed for biochemical investigation. For imaging, cells grown on glass coverslips were washed in PBS (five washes of 2 min each), fixed and permeabilized (in methanol for 7 min at -20°C), quenched (in PBS containing 1% BSA for 1 h at room temperature) and incubated with NeutrAvidin-Dylight 594 conjugated (for 1 h at room temperature). PAECs were rewashed (five washes of 2 min each), mounted on glass slides using ProLong Antifade reagent, examined and photographed using a Zeiss AxioImager M1 motorized upright microscope equipped with an AxioCam ICc1 R3 RGB color digital camera (Carl Zeiss MicroImaging, Inc., Thornwood, NY). For biochemical studies, control and transfected cells were lysed as above. The lysates were clarified by centrifugation to obtain a final supernatant expected to contain the biotinylated proteins internalized by control or transfected cells. The amounts of biotin-labeled protein were assessed by ELISA. For quantitative assessment of biotin molecules in the final PAEC supernatant, standard curves were generated using known concentrations of BSA-biotin. The average number of biotin molecules present in each cell lysate was determined for a series of decreasing concentrations using the linear part of a curve obtained by successively diluting a standard volume (100 µl) from each lysate, and normalized per mg of total protein.

Cell proliferation assay

Cell proliferation was determined using the Click-iT EdU Alexa Fluor Imaging kit according to the manufacturer's instructions. Briefly, control and transfected PAECs, grown on coverslips in 6-well plates (1.5×10^5 cells per well), were incubated in complete endothelial medium containing 10 µM EdU solution for 2 h at 37°C. PAECs were fixed with 3.7% formaldehyde in PBS and permeabilized with PBS containing 0.5% Triton X-100, then washed with 3% BSA in PBS before the Click-iT reaction cocktail was added to each well and incubated for 30 min, at room temperature. The coverslips were mounted using ProLong Antifade reagent with DAPI. EdU-positive cells were counted on high-power field of view images using a Zeiss AxioImager M1 motorized upright microscope equipped with an AxioCam ICc1 R3 RGB color digital camera and a 40x objective, and data were expressed as the ratio of EdU-positive cells to DAPI-stained cells per 50 high-power fields of view.

MTT assay

Triplicate aliquots of cells (10^6 cells suspended in 100 µl complete endothelial medium) were seeded onto a 96-well plate and serial dilutions were prepared in the endothelial medium. Cells were cultured for 48 h, followed by addition of 10 µl MTT Reagent to each well. After 5 h incubation, 100 µl of detergent was added to each well, the plate was covered and kept in the dark at room temperature overnight. Absorbance was measured at 595 nm using an Epoch BioTech microtiter plate reader (BioTech Instruments, Highland Park, VT) on the following day. Parallel triplicate experiments using non-treated PAECs were performed. A growth curve was generated to relate the OD_{595} values to the number of cells.

Flow cytometry analysis of cell cycle

The C-eGFP-EH_{ITSN}- and mCherry-SH3A–E_{ITSN}-transfected PAECs were harvested, washed with PBS and fixed in 75% ethanol at −20°C for 10 min followed by 15 min incubation at room temperature in 1 ml of 3 µM DAPI nucleic acid stain solution in staining buffer (100 mM Tris-HCl, pH 7.4, 150 mM NaCl, 1 mM $CaCl_2$, 0.5 mM $MgCl_2$ and 0.1% Nonidet P-40) followed by flow cytometry analysis of the cellular DNA content. Cell doublets were excluded using forward scatter area versus forward scatter height parameters. Gates for C-eGFP and mCherry expressing cells were drawn based on untransfected populations used as controls. At least 50,000 cells were collected for each sample and analyzed on a CytoFLEX flow cytometer (Beckman Coulter, Brea, CA). The proportion of cells within the synthetic (S) phase of the cell cycle was determined using DAPI, which binds to DNA in a stoichiometric manner. The population of G2 phase cells (having twice the DNA content of G1 phase cells), was defined as those cells that fluoresced twice as brightly as the G1 population. The S phase population was defined as the population of cells with fluorescence intensity between that of the G1 and the G2 populations. Cell doublets were gated out using PI (propidium iodide) area versus PI height, and PI intensity was measured on a linear scale. Kaluza software version 2.1 (Beckman Coulter, Brea, CA) was used to analyze the data.

PenNPF peptide treatment

PAECs grown on coverslips were incubated for 1 h with 12.5 µM PenNPF–FITC peptide using a 1 mg/ml stock solution of the peptide in PBS. After 1 h incubation, cells were washed with PBS and fixed in 4% paraformaldehyde before mounting on glass slides using Prolong Antifade reagent. Peptide uptake by PAECs was detected by fluorescence microscopy using a Zeiss AxioImager M1 motorized upright microscope equipped with an AxioCam ICc1 R3 RGB color digital camera and a 63x objective. Similarly, PAECs grown on 100 mm plates and transfected with myc-EH_{ITSN} were incubated for 12 h with PenNPF or control peptides (12.5 µM) as described by Clark and Petty (2010). Then, the cells were plated for the MTT assay. We generated the PenNPF peptide, which consisted of the membrane permeable Pen peptide (RQIKIWFQNRRMKWKK) (Derossi et al., 1996) followed by the NPF motif and vital residues for binding (PTGSSSTNPFL), as well as a FITC-tagged version (PenNPF–FITC) to facilitate morphological and biochemical detection. In addition, the following control peptides were used: (i) Pen-AAA (NPF residues substituted with an AAA sequence), (ii) Pen alone, (iii) NPF alone (NPF motif and the vital residues for binding) and (iv) Pen [scrambled] NPF peptide (the Pen peptide sequence and a scrambled NPF sequence).

PenNPF–FITC peptide overlay

The overlay assay was performed as described in Knezevic et al. (2011). Immediately following electrotransfer, nitrocellulose membranes containing PAEC lysates resolved by SDS–PAGE, were blocked for 1 h in blocking buffer [150 mM NaCl, 5% (w/v) non-fat powdered milk, 50 mM phosphate, pH 7.5], rinsed with water and incubated for 1 h in Buffer A (3% BSA, 0.1% TWEEN 20, 1 mM dithiothreitol and 20 mM Tris-HCl, pH 7.4) containing 5 µM PenNPF–FITC peptide per ml. The membranes were then washed in blocking buffer, rinsed with water, and incubated for 1 h in Buffer A (without dithiothreitol) containing anti-FITC antibody, followed by incubation the appropriate HRP-conjugated reporter antibody and ECL detection.

RNA isolation and RT-qPCR

Briefly, RNA from HPAECs was isolated using an RNeasy Micro Kit (Qiagen; Valencia, CA). RT-qPCR for *Xist* was performed on cDNA generated from 2000 ng of total RNA using a High-Capacity RNA to cDNA kit and Power SYBR Green PCR Master Mix (Thermo Fisher Scientific; Hanover Park, IL). Amplification and detection of specific products were performed using a Roche Light cycler 480 Detection System. Relative gene expression was calculated by comparing cycle times for each target PCR. The following human qPCR primer pairs (Sigma-Aldrich; St. Louis, MO) were used: *Xist*, fwd 5′-GGATGTCAAAAGATCGGCCC-3′, rev 5′-GTCCTCAGGTCTCACATGCT-3′; *ELK1*, fwd 5′-GCTGCCTCCTAGC-ATTTCACTTC-3′, rev 5′-CCACGCTGATAGAAGGGATGTG-3′; *KLF2*, fwd 5′-CCAAGAGTTCGCATCTGAAGGC-3′, rev 5′-CCGTGTGCTTT-CGGTAGTGGC-3′; *GAPDH* (used for mRNA normalization), fwd 5′-G-TCTCCTCTGACTTCAACAGCG-3′, rev 5′-ACCACCCTGTTGCTGTA-GCCAA-3′. Reactions were run under the following conditions: 95°C for 10 min; 95°C for 15 s then 60°C for 1 min, repeated 40 times; and the melting curve was 95°C for 15 s, 60°C for 1 min, 95°C for 15 s. Once the fluorescent signals were normalized to an internal reference, the threshold cycle (Ct) was set within the exponential phase of the reaction. Relative gene expression was expressed as a ΔCt value, and the comparative expression between treatments was subsequently calculated using the following equation: relative gene expression=$2^{-(\Delta Ct\ sample-\Delta Ct\ control)}$.

Luciferase reporter assay

Reporter constructs were generated by Origene (Rockville, MD). The human *Xist* cDNA clone was subcloned using SacI and XhoI restriction sites into the pmirGLO vector (Promega, Madison, WI). Controls and EH_{ITSN}-expressing ECs were co-transfected with the *Xist* reporter construct and a control Renilla construct, using Lipofectamine 3000 in 60 mm Petri dishes, according to the manufacturer's instructions. Cell lysates were obtained by adding Promega CCLR buffer (400 µl/plate), rocking the plates for 30 s to 1 min before scraping the monolayer. The resulting lysate was transferred to a chilled 1.5 ml microfuge tube on ice. After a short centrifugation (12,000 ***g*** for 1 min at 4°C), the supernatant was stored at −80°C until readings were taken. The firefly and Renilla luciferase activities were determined using a double Luciferase Reporter Analysis System (Promega) according to the manufacturer's instructions. The relative luciferase activity was calculated based on the firefly/Renilla fluorescence ratio.

ELK1 activity assay

Nuclear extracts of control and transfected cells were prepared using the NE-PER Nuclear and Cytoplasmic Extraction kit (Thermo Fisher Scientific) according to the manufacturer's protocol. The nuclear extracts were then analyzed using a TransAM Elk-1 ELISA kit (Active Motif, Carlsbad, CA) in a 96-well plate containing the immobilized Elk1 consensus site oligonucleotide as reported by Patel et al. (2013). Activated Elk1 was detected using an antibody against phosphorylated Elk1 followed by an HRP-conjugated reporter antibody. The plates were read at 450 nm using an Epoch plate reader. Data from triplicate wells in three different experiments were expressed as a mean±s.d.

Statistical analysis

All experiments were repeated at least three times, and statistical analyses were performed using GraphPad Prism 8.2.1 software. Student's *t*-test (two tailed, unpaired *t*-tests) and one-way analysis of variance (ANOVA) were used to compare the samples and their controls. All data are expressed as mean±s.d. A value of $P<0.05$ was considered significant.

Acknowledgements

The authors thank Drs Serpil Erzurum and Suzy Comhair (Lerner Research Institute, CCLCM Cleveland Clinic; HL60917) and the Pulmonary Hypertension Breakthrough Initiative (PHBI) for providing the pulmonary artery endothelial cells isolated from PAH patients and non-disease controls. Funding for the PHBI is provided under an NHLBI R24 grant, #R24HL123767, and by the Cardiovascular Medical Research and Education Fund (CMREF).

Competing interests

The authors declare no competing or financial interests.

Author contributions

Conceptualization: S.A.P., D.N.P.; Methodology: S.A.P., S.Q., D.N.P.; Formal analysis: D.N.P.; Investigation: S.Q., M.P., P.D., B.G.; Resources: S.A.P.; Writing - original draft: D.N.P.; Writing - review & editing: S.A.P.; Visualization: D.N.P.; Supervision: S.A.P., D.N.P.; Project administration: S.A.P.; Funding acquisition: S.A.P.

Funding

This work was supported by National Institutes of Health R01 HL127022 to S.A.P. Deposited in PMC for release after 12 months.

Supplementary information

Supplementary information available online at
http://jcs.biologists.org/lookup/doi/10.1242/jcs.237776.supplemental

Peer review history

The peer review history is available online at
https://jcs.biologists.org/lookup/doi/10.1242/jcs.237776.reviewer-comments.pdf

References

Addis, R., Campesi, I., Fois, M., Capobianco, G., Dessole, S., Fenu, G., Montella, A., Cattaneo, M. G., Vicentini, L. M. and Franconi, F. (2014). Human umbilical endothelial cells (HUVECs) have a sex: characterisation of the phenotype of male and female cells. *Biol. Sex. Differ.* **5**, 18. doi:10.1186/s13293-014-0018-2

Alvisi, G., Paolini, L., Contarini, A., Zambarda, C., Di Antonio, V., Colosini, A., Mercandelli, N., Timmoneri, M., Palù, G., Caimi, L. et al. (2018). Intersectin goes nuclear: secret life of an endocytic protein. *Biochem. J.* **475**, 1455-1472. doi:10.1042/BCJ20170897

Atkins, G. B. and Jain, M. K. (2007). Role of Krüppel-like transcription factors in endothelial biology. *Circ. Res.* **100**, 1686-1695. doi:10.1161/01.RES.0000267856.00713.0a

Awad, K. S., West, J. D., de Jesus Perez, V. and Maclean, M. (2016). Novel signaling pathways in pulmonary arterial hypertension (2015 Grover Conference Series). *Pulm. Circ.* **6**, 285-294. doi:10.1086/688034

Bardita, C., Predescu, D., Justice, M. J., Petrache, I. and Predescu, S. (2013). In vivo knockdown of intersectin-1s alters endothelial cell phenotype and causes microvascular remodeling in the mouse lungs. *Apoptosis* **18**, 57-76. doi:10.1007/s10495-012-0762-x

Barnes, J. W., Tian, L., Heresi, G. A., Farver, C. F., Asosingh, K., Comhair, S. A. A., Aulak, K. S. and Dweik, R. A. (2015). O-linked β-N-acetylglucosamine transferase directs cell proliferation in idiopathic pulmonary arterial hypertension. *Circulation* **131**, 1260-1268. doi:10.1161/CIRCULATIONAHA.114.013878

Borlido, J., Zecchini, V. and Mills, I. G. (2009). Nuclear trafficking and functions of endocytic proteins implicated in oncogenesis. *Traffic* **10**, 1209-1220. doi:10.1111/j.1600-0854.2009.00922.x

Boucherat, O., Chabot, S., Paulin, R., Trinh, I., Bourgeois, A., Potus, F., Lampron, M.-C., Lambert, C., Breuils-Bonnet, S., Nadeau, V. et al. (2017). HDAC6: a novel histone deacetylase implicated in pulmonary arterial hypertension. *Sci. Rep.* **7**, 4546. doi:10.1038/s41598-017-04874-4

Brash, L., Barnes, G. D., Brewis, M. J., Church, A. C., Gibbs, S. J., Howard, L. S. G. E., Jayasekera, G., Johnson, M. K., Mcglinchey, N., Onorato, J. et al. (2018). Short-term hemodynamic effects of apelin in patients with pulmonary arterial hypertension. *JACC Basic Transl. Sci.* **3**, 176-186. doi:10.1016/j.jacbts.2018.01.013

Carman, B. L., Predescu, D. N., Machado, R. and Predescu, S. A. (2019). Plexiform arteriopathy in rodent models of pulmonary arterial hypertension. *Am. J. Pathol.* **189**, 1133-1144. doi:10.1016/j.ajpath.2019.02.005

Chelladurai, P., Seeger, W. and Pullamsetti, S. S. (2012). Matrix metalloproteinases and their inhibitors in pulmonary hypertension. *Eur. Respir. J.* **40**, 766-782. doi:10.1183/09031936.00209911

Clark, A. J. and Petty, H. R. (2010). A cell permeant peptide containing the cytoplasmic tail sequence of Fc receptor type IIA reduces calcium signaling and phagolysosome formation in neutrophils. *Cell. Immunol.* **261**, 153-158. doi:10.1016/j.cellimm.2009.12.002

Comhair, S. A. A., Xu, W., Mavrakis, L., Aldred, M. A., Asosingh, K. and Erzurum, S. C. (2012). Human primary lung endothelial cells in culture. *Am. J. Respir. Cell Mol. Biol.* **46**, 723-730. doi:10.1165/rcmb.2011-0416TE

de Beer, T., Carter, R. E., Lobel-Rice, K. E., Sorkin, A. and Overduin, M. (1998). Structure and Asn-Pro-Phe binding pocket of the Eps15 homology domain. *Science* **281**, 1357-1360. doi:10.1126/science.281.5381.1357

Derossi, D., Calvet, S., Trembleau, A., Brunissen, A., Chassaing, G. and Prochiantz, A. (1996). Cell internalization of the third helix of the Antennapedia homeodomain is receptor-independent. *J. Biol. Chem.* **271**, 18188-18193. doi:10.1074/jbc.271.30.18188

Dorfmuller, P., Perros, F., Balabanian, K. and Humbert, M. (2003). Inflammation in pulmonary arterial hypertension. *Eur. Respir. J.* **22**, 358-363. doi:10.1183/09031936.03.00038903

Eichstaedt, C. A., Song, J., Viales, R. R., Pan, Z., Benjamin, N., Fischer, C., Hoeper, M. M., Ulrich, S., Hinderhofer, K. and Grünig, E. (2017). First identification of Krüppel-like factor 2 mutation in heritable pulmonary arterial hypertension. *Clin. Sci. (Lond.)* **131**, 689-698. doi:10.1042/CS20160930

Elinoff, J. M., Rame, J. E., Forfia, P. R., Hall, M. K., Sun, J., Gharib, A. M., Abd-Elmoniem, K., Graninger, G., Harper, B., Danner, R. L. et al. (2013). A pilot study of the effect of spironolactone therapy on exercise capacity and endothelial dysfunction in pulmonary arterial hypertension: study protocol for a randomized controlled trial. *Trials* **14**, 91. doi:10.1186/1745-6215-14-91

Fang, J., Sun, C.-C. and Gong, C. (2016). Long noncoding RNA XIST acts as an oncogene in non-small cell lung cancer by epigenetically repressing KLF2 expression. *Biochem. Biophys. Res. Commun.* **478**, 811-817. doi:10.1016/j.bbrc.2016.08.030

Ferreiro, I., Barragan, M., Gubern, A., Ballestar, E., Joaquin, M. and Posas, F. (2010). The p38 SAPK is recruited to chromatin via its interaction with transcription factors. *J. Biol. Chem.* **285**, 31819-31828. doi:10.1074/jbc.M110.155846

Gardiner, K., Davisson, M. T. and Crnic, L. S. (2004). Building protein interaction maps for Down's syndrome. *Brief. Funct. Genomic. Proteomic.* **3**, 142-156. doi:10.1093/bfgp/3.2.142

Ghouleh, I. A., Sahoo, S., Meijles, D. N., Amaral, J. H., DE Jesus, D. S., Sembrat, J., Rojas, M., Goncharov, D. A., Goncharova, E. A. and Pagano, P. J. (2017). Endothelial Nox1 oxidase assembly in human pulmonary arterial hypertension; driver of Gremlin1-mediated proliferation. *Clin. Sci. (Lond.)* **131**, 2019-2035. doi:10.1042/CS20160812

Gu, F., Zhang, H., Qin, F., Liu, X., Li, W., Fu, L., Ying, G., Li, B., Zhang, M. and Ma, Y. (2015). Intersectin1-S, a multidomain adapter protein, is essential for malignant glioma proliferation. *Glia* **63**, 1595-1605. doi:10.1002/glia.22830

Harris, J., Herrero-Garcia, E., Russo, A., Kajdacsy-Balla, A., O'Bryan, J. P. and Chiu, B. (2017). Silencing intersectin 1 slows orthotopic neuroblastoma growth in mice. *J. Pediatr. Hematol. Oncol.* **39**, e413-e418. doi:10.1097/MPH.0000000000000931

Hassoun, P. M., Mouthon, L., Barberà, J. A., Eddahibi, S., Flores, S. C., Grimminger, F., Jones, P. L., Maitland, M. L., Michelakis, E. D., Morrell, N. W. et al. (2009). Inflammation, growth factors, and pulmonary vascular remodeling. *J. Am. Coll. Cardiol.* **54**, S10-S19. doi:10.1016/j.jacc.2009.04.006

Hemnes, A. R., Rathinasabapathy, A., Austin, E. A., Brittain, E. L., Carrier, E. J., Chen, X., Fessel, J. P., Fike, C. D., Fong, P., Fortune, N. et al. (2018). A potential therapeutic role for angiotensin-converting enzyme 2 in human pulmonary arterial hypertension. *Eur. Respir. J.* **51**, 1702638. doi:10.1183/13993003.02638-2017

Hirashiki, A., Adachi, S., Nakano, Y., Kamimura, Y., Ogo, T., Nakanishi, N., Morisaki, T., Morisaki, H., Shimizu, A., Toba, K. et al. (2017). Left main coronary artery compression by a dilated main pulmonary artery and left coronary sinus of Valsalva aneurysm in a patient with heritable pulmonary arterial hypertension and FLNA mutation. *Pulm. Circ.* **7**, 734-740. doi:10.1177/2045893217716107

Hood, K. Y., Montezano, A. C., Harvey, A. P., Nilsen, M., Maclean, M. R. and Touyz, R. M. (2016). Nicotinamide adenine dinucleotide phosphate oxidase-mediated redox signaling and vascular remodeling by 16α-hydroxyestrone in human pulmonary artery cells: implications in pulmonary arterial hypertension. *Hypertension* **68**, 796-808. doi:10.1161/HYPERTENSIONAHA.116.07668

Huang, L., Li, L., Hu, E., Chen, G., Meng, X., Xiong, C. and He, J. (2018). Potential biomarkers and targets in reversibility of pulmonary arterial hypertension secondary to congenital heart disease: an explorative study. *Pulm. Circ.* **8**, 2045893218755987. doi:10.1177/2045893218755987

Hunter, M. P., Russo, A. and O'Bryan, J. P. (2013). Emerging roles for intersectin (ITSN) in regulating signaling and disease pathways. *Int. J. Mol. Sci.* **14**, 7829-7852. doi:10.3390/ijms14047829

Hussain, N. K., Yamabhai, M., Ramjaun, A. R., Guy, A. M., Baranes, D., O'Bryan, J. P., Der, C. J., Kay, B. K. and Mcpherson, P. S. (1999). Splice variants of intersectin are components of the endocytic machinery in neurons and nonneuronal cells. *J. Biol. Chem.* **274**, 15671-15677. doi:10.1074/jbc.274.22.15671

Jakob, B., Kochlamazashvili, G., Jäpel, M., Gauhar, A., Bock, H. H., Maritzen, T. and Haucke, V. (2017). Intersectin 1 is a component of the Reelin pathway to regulate neuronal migration and synaptic plasticity in the hippocampus. *Proc. Natl. Acad. Sci. USA* **114**, 5533-5538. doi:10.1073/pnas.1704447114

Jeganathan, N., Predescu, D., Zhang, J., Sha, F., Bardita, C., Patel, M., Wood, S., Borgia, J. A., Balk, R. A. and Predescu, S. (2016). Rac1-mediated cytoskeleton rearrangements induced by intersectin-1s deficiency promotes lung cancer cell proliferation, migration and metastasis. *Mol. Cancer* **15**, 59. doi:10.1186/s12943-016-0543-1

Jeganathan, N., Predescu, D. and Predescu, S. (2017). Intersectin-1s deficiency in pulmonary pathogenesis. *Respir. Res.* **18**, 168. doi:10.1186/s12931-017-0652-4

Juntilla, M. M. and Koretzky, G. A. (2008). Critical roles of the PI3K/Akt signaling pathway in T cell development. *Immunol. Lett.* **116**, 104-110. doi:10.1016/j.imlet.2007.12.008

Keating, D. J., Chen, C. and Pritchard, M. A. (2006). Alzheimer's disease and endocytic dysfunction: clues from the Down syndrome-related proteins, DSCR1 and ITSN1. *Ageing Res. Rev.* **5**, 388-401. doi:10.1016/j.arr.2005.11.001

Kim, J. (2014). Apelin-APJ signaling: a potential therapeutic target for pulmonary arterial hypertension. *Mol. Cells* **37**, 196-201. doi:10.14348/molcells.2014.2308

Kim, J., Hwangbo, C., Hu, X., Kang, Y., Papangeli, I., Mehrotra, D., Park, H., Ju, H., Mclean, D. L., Comhair, S. A. et al. (2015). Restoration of impaired endothelial myocyte enhancer factor 2 function rescues pulmonary arterial hypertension. *Circulation* **131**, 190-199. doi:10.1161/CIRCULATIONAHA.114.013339

Knezevic, I., Predescu, D., Bardita, C., Wang, M., Sharma, T., Keith, B., Neamu, R., Malik, A. B. and Predescu, S. (2011). Regulation of dynamin-2 assembly-disassembly and function through the SH3A domain of intersectin-1s. *J. Cell. Mol. Med.* **15**, 2364-2376. doi:10.1111/j.1582-4934.2010.01226.x

Kropyvko, S., Gerasymchuk, D., Skrypkina, I., Dergai, M., Dergai, O., Nikolaienko, O., Rynditch, A. and Tsyba, L. (2010). Structural diversity and differential expression of novel human intersectin 1 isoforms. *Mol. Biol. Rep.* **37**, 2789-2796. doi:10.1007/s11033-009-9824-8

Li, G., Liu, Y., Zhu, Y., Liu, A., Xu, Y., Li, X., Li, Z., Su, J. and Sun, L. (2013). ACE2 activation confers endothelial protection and attenuates neointimal lesions in prevention of severe pulmonary arterial hypertension in rats. *Lung* **191**, 327-336. doi:10.1007/s00408-013-9470-8

Libert, C., Dejager, L. and Pinheiro, I. (2010). The X chromosome in immune functions: when a chromosome makes the difference. *Nat. Rev. Immunol.* **10**, 594-604. doi:10.1038/nri2815

Loeb, C. R. K., Harris, J. L. and Craik, C. S. (2006). Granzyme B proteolyzes receptors important to proliferation and survival, tipping the balance toward apoptosis. *J. Biol. Chem.* **281**, 28326-28335. doi:10.1074/jbc.M604544200

McLean, D. L., Kim, J., Kang, Y., Shi, H., Atkins, G. B., Jain, M. K. and Chun, H. J. (2012). Apelin/APJ signaling is a critical regulator of statin effects in vascular endothelial cells—brief report. *Arterioscler. Thromb. Vasc. Biol.* **32**, 2640-2643. doi:10.1161/ATVBAHA.112.300317

Milletti, F. (2012). Cell-penetrating peptides: classes, origin, and current landscape. *Drug Discov. Today* **17**, 850-860. doi:10.1016/j.drudis.2012.03.002

Okamoto, M., Schoch, S. and Südhof, T. C. (1999). EHSH1/intersectin, a protein that contains EH and SH3 domains and binds to dynamin and SNAP-25. A protein connection between exocytosis and endocytosis? *J. Biol. Chem.* **274**, 18446-18454. doi:10.1074/jbc.274.26.18446

Patel, M., Predescu, D., Tandon, R., Bardita, C., Pogoriler, J., Bhorade, S., Wang, M., Comhair, S., Ryan-Hemnes, A., Chen, J. et al. (2013). A novel p38 mitogen-activated protein kinase/Elk-1-dependent molecular mechanism underlying abnormal endothelial cell proliferation in plexogenic pulmonary arterial hypertension. *J. Biol. Chem.* **288**, 25701-25716. doi:10.1074/jbc.M113.502674

Patel, M., Predescu, D., Bardita, C., Chen, J., Jeganathan, N., Pritchard, M., Dibartolo, S., Machado, R. and Predescu, S. (2017). Modulation of Intersectin-1s Lung Expression Induces Obliterative Remodeling and Severe Plexiform Arteriopathy in the Murine Pulmonary Vascular Bed. *Am. J. Pathol.* **187**, 528-542. doi:10.1016/j.ajpath.2016.11.012

Predescu, S. A., Predescu, D. N., Timblin, B. K., Stan, R. V. and Malik, A. B. (2003). Intersectin regulates fission and internalization of caveolae in endothelial cells. *Mol. Biol. Cell* **14**, 4997-5010. doi:10.1091/mbc.e03-01-0041

Predescu, D. N., Neamu, R., Bardita, C., Wang, M. and Predescu, S. A. (2012). Impaired caveolae function and upregulation of alternative endocytic pathways induced by experimental modulation of intersectin-1s expression in mouse lung endothelium. *Biochem. Res. Int.* **2012**, 672705. doi:10.1155/2012/672705

Predescu, D., Qin, S., Patel, M., Bardita, C., Bhalli, R. and Predescu, S. (2018). Epsin15 homology domains: role in the pathogenesis of pulmonary arterial hypertension. *Front. Physiol.* **9**, 1393. doi:10.3389/fphys.2018.01393

Predescu, S. A., Carman, B., Qin, S. and Predescu, D. N. (2019). The EH-induced mouse model of pulmonary arterial hypertension recapitulates gender differences of human disease. *Am. J. Respir. Crit. Care. Med.* **199**, A5290. doi:10.1164/ajrccm-conference.2019.199.1_MeetingAbstracts.A5290

Pucharcos, C., Casas, C., Nadal, M., Estivill, X. and de la Luna, S. (2001). The human intersectin genes and their spliced variants are differentially expressed. *Biochim. Biophys. Acta* **1521**, 1-11. doi:10.1016/S0167-4781(01)00276-7

Russo, A., Okur, M. N., Bosland, M. and O'bryan, J. P. (2015). Phosphatidylinositol 3-kinase, class 2 beta (PI3KC2β) isoform contributes to neuroblastoma tumorigenesis. *Cancer Lett.* **359**, 262-268. doi:10.1016/j.canlet.2015.01.026

Sanchez, O., Marcos, E., Perros, F., Fadel, E., Tu, L., Humbert, M., Dartevelle, P., Simonneau, G., Adnot, S. and Eddahibi, S. (2007). Role of endothelium-derived CC chemokine ligand 2 in idiopathic pulmonary arterial hypertension. *Am. J. Respir. Crit. Care. Med.* **176**, 1041-1047. doi:10.1164/rccm.200610-1559OC

Schurz, H., Salie, M., Tromp, G., Hoal, E. G., Kinnear, C. J. and Möller, M. (2019). The X chromosome and sex-specific effects in infectious disease susceptibility. *Hum. Genomics* **13**, 2. doi:10.1186/s40246-018-0185-z

Sengar, A. S., Ellegood, J., Yiu, A. P., Wang, H., Wang, W., Juneja, S. C., Lerch, J. P., Josselyn, S. A., Henkelman, R. M., Salter, M. W. et al. (2013). Vertebrate intersectin1 is repurposed to facilitate cortical midline connectivity and higher order cognition. *J. Neurosci.* **33**, 4055-4065. doi:10.1523/JNEUROSCI.4428-12.2013

Shah, T., Qin, S., Vashi, M., Predescu, D. N., Jeganathan, N., Bardita, C., Ganesh, B., Dibartolo, S., Fogg, L. F., Balk, R. A. et al. (2018). Alk5/Runx1

signaling mediated by extracellular vesicles promotes vascular repair in acute respiratory distress syndrome. *Clin. Transl. Med.* **7**, 19. doi:10.1186/s40169-018-0197-2

Shenoda, B. B., Tian, Y., Alexander, G. M., Aradillas-Lopez, E., Schwartzman, R. J. and Ajit, S. K. (2018). miR-34a-mediated regulation of XIST in female cells under inflammation. *J. Pain Res.* **11**, 935-945. doi:10.2147/JPR.S159458

Stacher, E., Graham, B. B., Hunt, J. M., Gandjeva, A., Groshong, S. D., Mclaughlin, V. V., Jessup, M., Grizzle, W. E., Aldred, M. A., Cool, C. D. et al. (2012). Modern age pathology of pulmonary arterial hypertension. *Am. J. Respir. Crit. Care. Med.* **186**, 261-272. doi:10.1164/rccm.201201-0164OC

Tiede, S. L., Wassenberg, M., Christ, K., Schermuly, R. T., Seeger, W., Grimminger, F., Ghofrani, H. A. and Gall, H. (2016). Biomarkers of tissue remodeling predict survival in patients with pulmonary hypertension. *Int. J. Cardiol.* **223**, 821-826. doi:10.1016/j.ijcard.2016.08.240

Tong, X.-K., Hussain, N. K., Adams, A. G., O'Bryan, J. P. and McPherson, P. S. (2000a). Intersectin can regulate the Ras/MAP kinase pathway independent of its role in endocytosis. *J. Biol. Chem.* **275**, 29894-29899. doi:10.1074/jbc.M004096200

Tong, X.-K., Hussain, N. K., DE Heuvel, E., Kurakin, A., Abi-Jaoude, E., Quinn, C. C., Olson, M. F., Marais, R., Baranes, D., Kay, B. K. et al. (2000b). The endocytic protein intersectin is a major binding partner for the Ras exchange factor mSos1 in rat brain. *EMBO J.* **19**, 1263-1271. doi:10.1093/emboj/19.6.1263

Tuder, R. M., Groves, B., Badesch, D. B. and Voelkel, N. F. (1994). Exuberant endothelial cell growth and elements of inflammation are present in plexiform lesions of pulmonary hypertension. *Am. J. Pathol.* **144**, 275-285.

Vacca, M., Della Ragione, F., Scalabrì, F. and D'Esposito, M. (2016). X inactivation and reactivation in X-linked diseases. *Semin. Cell Dev. Biol.* **56**, 78-87. doi:10.1016/j.semcdb.2016.03.009

Wang, X. M., Shi, K., Li, J. J., Chen, T. T., Guo, Y. H., Liu, Y. L., Yang, Y. F. and Yang, S. (2015). Effects of angiotensin II intervention on MMP-2, MMP-9, TIMP-1, and collagen expression in rats with pulmonary hypertension. *Genet. Mol. Res.* **14**, 1707-1717. doi:10.4238/2015.March.6.17

Wang, J., Syrett, C. M., Kramer, M. C., Basu, A., Atchison, M. L. and Anguera, M. C. (2016). Unusual maintenance of X chromosome inactivation predisposes female lymphocytes for increased expression from the inactive X. *Proc. Natl. Acad. Sci. USA* **113**, E2029-E2038. doi:10.1073/pnas.1520113113

Wu, W., Xiao, H., Laguna-Fernandez, A., Villarreal, G., Jr, Wang, K.-C., Geary, G. G., Zhang, Y., Wang, W.-C., Huang, H.-D., Zhou, J. et al. (2011). Flow-dependent regulation of Krüppel-like factor 2 is mediated by microRNA-92a. *Circulation* **124**, 633-641. doi:10.1161/CIRCULATIONAHA.110.005108

Xu, T., Jiang, W., Fan, L., Gao, Q. and Li, G. (2017). Upregulation of long noncoding RNA Xist promotes proliferation of osteosarcoma by epigenetic silencing of P21. *Oncotarget* **8**, 101406-101417. doi:10.18632/oncotarget.20738

Yang, P., Read, C., Kuc, R. E., Buonincontri, G., Southwood, M., Torella, R., Upton, P. D., Crosby, A., Sawiak, S. J., Carpenter, T. A. et al. (2017). Elabela/Toddler Is an endogenous agonist of the Apelin APJ receptor in the adult cardiovascular system, and exogenous administration of the peptide compensates for the downregulation of its expression in pulmonary arterial hypertension. *Circulation* **135**, 1160-1173. doi:10.1161/CIRCULATIONAHA.116.023218

Yang, Z., Jiang, X., Jiang, X. and Zhao, H. (2018). X-inactive-specific transcript: a long noncoding RNA with complex roles in human cancers. *Gene* **679**, 28-35. doi:10.1016/j.gene.2018.08.071

Yang, P., Read, C., Kuc, R. E., Nyimanu, D., Williams, T. L., Crosby, A., Buonincontri, G., Southwood, M., Sawiak, S. J., Glen, R. C. et al. (2019). A novel cyclic biased agonist of the apelin receptor, MM07, is disease modifying in the rat monocrotaline model of pulmonary arterial hypertension. *Br. J. Pharmacol.* **176**, 1206-1221. doi:10.1111/bph.14603

Yu, S., Hong, Q., Wang, Y., Hou, K., Wang, L., Zhang, Y., Fu, B., Zhou, Y., Zheng, W., Chen, X. et al. (2015). High concentrations of uric acid inhibit angiogenesis via regulation of the Krüppel-like factor 2-vascular endothelial growth factor-A axis by miR-92a. *Circ. J.* **79**, 2487-2498. doi:10.1253/circj.CJ-15-0283

Zhang, W. and Liu, H. T. (2002). MAPK signal pathways in the regulation of cell proliferation in mammalian cells. *Cell Res.* **12**, 9-18. doi:10.1038/sj.cr.7290105

Zhang, Y., Dong, X., Shirazi, J., Gleghorn, J. P. and Lingappan, K. (2018). Pulmonary endothelial cells exhibit sexual dimorphism in their response to hyperoxia. *Am. J. Physiol. Heart Circ. Physiol.* **315**, H1287-H1292. doi:10.1152/ajpheart.00416.2018